

CHAPTER 20

RADIATION EFFECTS ON DNA: THEORETICAL INVESTIGATIONS OF ELECTRON, HOLE AND EXCITATION PATHWAYS TO DNA DAMAGE

ANIL KUMAR AND MICHAEL D. SEVILLA*

Department of Chemistry, Oakland University, Rochester, Michigan 48309, USA

Abstract: Radiation induced DNA damage is the most significant biological effect of radiation. Initially, radiation interacts with each component of DNA randomly resulting in DNA holes, electrons and excited states. Holes and electrons undergo rapid transfer to the most stable sites followed by proton transfer processes. These initial effects depend on the fundamental properties of DNA such as ionization potentials and electron affinities which are amenable to high level ab initio theories such as density functional theory. In this review, the recent theoretical treatments of these likely radiation intermediates are discussed. Topics include DNA base and base pair electron affinities, ionization potentials, proton transfer processes, solvation effects on the electron affinity of bases and base pairs, the role of low energy electrons (LEEs) in DNA damage, and sugar radical formation from hole excited states. These results clearly show a role for molecular orbital theories in developing a full explanation of the radiation damage processes

Keywords: Radiation Induced Damage, Ionization Potential, Electron Affinity (EA), Low Energy Electron (LEE), Strand Breaks, Solvation of DNA Bases, Guanine Radical Cation (G^{*+}), TD-DFT Study

20.1. INTRODUCTION

Exposure of living systems to ionizing radiation results in a wide assortment of lesions the most significant of is damage to genomic DNA. Mechanisms that lead to specific radiation induced DNA damage are of intense research interest [1–8]. Initially radiation ionizes each component of DNA, i.e., bases, sugar-phosphate backbone and the surrounding water molecules randomly resulting in many secondary electrons. Most of the secondary electrons produced are low energy

* Corresponding author, email: sevilla@oakland.edu

electrons (LEE) in the 0–15 eV range [8–10]. Recently, these LEEs have been found to result in a specific damage to DNA by bond rupture [10–16] chiefly through dissociative electron attachment (DEA) mechanisms. However, most electrons ultimately thermalize and either recombine with holes or are captured by the DNA bases of highest electron affinity, i.e., the pyrimidine bases (thymine and cytosine) [17–18] forming anion radicals. The holes (cation radicals) produced in the ionization event in DNA migrate through the DNA to the sites of lowest ionization energy [18–21]. Among the four DNA bases (adenine (A), thymine (T), guanine (G) and cytosine (C)) guanine base has the lowest ionization potential (IP) [2, 3, 22–25] and because of this property guanine acts as the predominant hole acceptor site in DNA. Holes initially created on sugar-phosphate may undergo two competitive reactions: (i) deprotonation of the sugar cation radical to form neutral sugar radicals and (ii) hole transfer to the nearest DNA base [2, 26].

Recently, it has been reported that irradiation of DNA by a high-energy Argon ion-beam [27, 28] (high linear energy transfer, LET, radiation) produced a far greater yield of sugar radicals than was found by γ -irradiation (a low LET radiation). The sugar radical formation is of interest in DNA as these species directly lead to DNA strand breaks and DNA strand breaks are among the most biologically important lesions. Since these sugar radicals were formed predominantly along the ion track, where ionizations and excitations are in proximity, it was proposed that excited state cation radicals could be the direct precursors of the neutral sugar radicals [27, 28]. Visible photoexcitation of the guanine radical cation ($G^{\bullet+}$) in DNA and in the model compounds of deoxyribonucleosides and deoxyribonucleotides gave a high yields of deoxyribose sugar radical formation [29] which confirmed the proposed hypothesis [27, 28]. Such track structure dependent phenomenon are especially significant in the formation of the most lethal type of damage, the double strand break from multiple damage sites (MDS). When several DNA damages are produced in close proximity on both DNA strands, double strand breaks arise which are resistant to repair enzymes because of the loss of local structural information. For this reason high LET radiations (α -particles, atom ion beams, neutrons) are far more biologically damaging by ca. 10 fold than low LET radiations such as β -particles, X-rays and γ -rays.

The overview described above clearly shows that DNA damage processes are complex but all stem from the initial ionization and excitation events. Owing to the simplicity of the initial events ionization and electron addition a detailed understanding of these initial steps are amenable to treatment by first principles. In recent years, as a result of the ready access to substantial computational resources these initial mechanisms have been addressed using sophisticated *ab initio* (Hartree-Fock (HF), Møller-Plesset perturbation theory (MP2)) and the density functional (DFT) methods [30, 31]. These theoretical predictions when combined with experimental results give considerable insight and in depth understanding of the mechanisms of DNA damage. Experimental results become better understood when theoretical modeling allows for new interpretations and suggestions for further experiments arise. In this review, we will discuss our recent efforts employing theory to aid

our understanding of DNA base and sugar radical formation, DNA base electron affinities and ionization potentials, the effect of base-pairing and proton transfer, processes induced by excited states of DNA base radical cations in nucleosides and dinucleosides, interaction of LEEs with nucleotides leading to strand breaks and finally, the preferred states of protonation and tautomerization in the guanosine radical cation.

20.2. GROUND STATE ION RADICAL FORMATION

Formation of ion radicals, i.e., cation and anion radicals, as a result of high energy radiation is a primary step in DNA damage by direct mechanisms. Therefore, it has long been recognized that knowledge of ionization potentials (IPs) and electron affinities (EAs) of DNA bases (A, T, G and C), sugar and phosphate is of fundamental importance. Structures of DNA and bases (A, T, G and C) and RNA base (uracil (U)) are shown in Figure 20-1. It has been known from electron spin resonance (ESR) studies of γ -irradiated DNA at low temperature, that the purine cations (mainly $G^{\bullet+}$ and small amounts of $A^{\bullet+}$) and pyrimidine anions ($T^{\bullet-}$ and $C^{\bullet-}$ roughly in equal amounts initially) were trapped in DNA [32]. In addition to IPs and EAs, theoretical calculations were performed to fully understand the molecular structure of radicals, the nature of hole and electron localization and spin density distribution within the molecule.

20.2.1. Ionization Potential of DNA Bases and Base Pairs

Gas phase ionization potentials (IPs) of DNA bases, guanine, adenine, thymine and cytosine, have been calculated using a variety of levels of theory [33–40]. In Table 20-1, we compare representative theoretical values with available

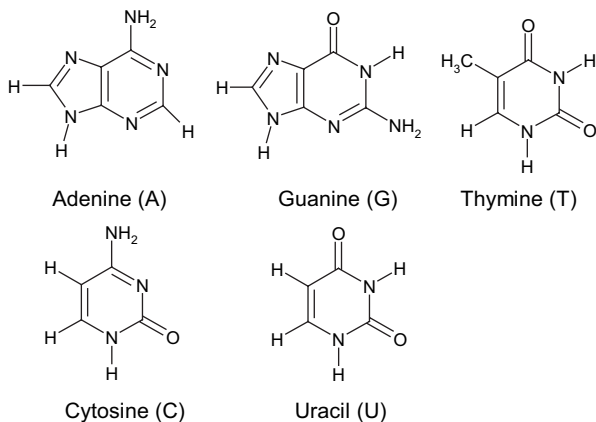


Figure 20-1. Structures of adenine (A), guanine (G), thymine (T), cytosine (C) and uracil (U)

Table 20-1. Gas phase Ionization potential (eV) of DNA bases calculated using different theoretical methods

Method	Refs.	Guanine		Adenine		Cytosine		Thymine	
		IP _{adia}	IP _{vert}						
MP2/6-31+G(d) ^a	33	7.66	8.04	8.18	8.58	8.74	8.82	8.85	(10.33)
B3LYP/TZVP	34	7.66		8.09		8.57		8.76	
B3LYP/6-11++G**	34	7.68		8.12		8.59		8.76	
B3LYP/6-311+G(3df, p)	35	7.64		8.09		8.57		8.74	
CCSD(T)/6-311++G(2df, 2p)	37			8.25		8.71			
B3-PMP2/6-311++G(3df, 2p)	37			8.28		8.43		8.79	
MP2/6-31G(2d(0.8, α_d), p) ^b	38	7.75	8.21	8.23	8.63	8.78	9.07	8.87	9.13
PMP2/6-31++G(d,p)	39	7.90	8.33	8.23	8.62	8.78	8.69	8.74	9.07
Experiment	41,42	7.77	8.24	8.26	8.44	8.68	8.94	8.87	9.14

^aGeometries were optimized at HF/6-31G* level [33]; ^bThe optimal value of $\alpha_d = 0.1$ was considered [38].

experimental data [41–43]. Using the MP2/6-31+G(d)//HF/6-31G* method, Colson et al. [33] calculated the gas phase adiabatic ionization potential (IP_{adia}) of G, A, C and T, which were found to lie within 0.1 eV of the experimental values (Table 20-1). The vertical ionization potentials (IP_{vert}) are also calculated within 0.2 eV except thymine, which had a difference of 1.2 eV; however, subsequent calculations of the IP_{vert} of thymine by other workers (Table 20-1) show an excellent agreement with experiment [38, 39]. Using photodetachment-photoelectron (PD-PE) spectroscopy, Yang et al. [43] recently found the ionization potentials (IPs) of nucleotide anions and observed that 2'-deoxyguanosine 5'-monophosphate has a lower IP than the other three DNA nucleotides as would be expected from the DNA bases IPs. More recent calculations find values in excellent agreement with experiment by the use of extended basis sets and higher level of theories, such as electron propagator calculation by Ortiz et al. [37–40]. From Table 20-1, we see that experimental order of the ionization potential $G < A < C < T$ is very well predicted by the theory.

Since DNA damage in a biological system occurs in aqueous environments, the effect of aqueous solvent on the ionization energies of the DNA components needs to be considered. The ionization thresholds energy of nucleotide anions in aqueous solution has been estimated from gas-phase photoelectron experiments, combined with results from self-consistent field (SCF) and post-SCF MO calculation and with theoretical Gibbs free energy of hydration by LeBreton et al. [44]. They [44] showed that the solvation has pronounced effect and lowers the ionization potential of the nucleobases by several eVs below the gas-phase values [41, 42]. Using polarized continuum model (PCM) with water as solvent ($\epsilon = 78.4$) the B3LYP/6-31++G(d,p) calculation was carried out by Close [45]. After solvation energy correction of the electron, the ionization potentials of G, A, C and T were found to be 4.71 eV, 5.05 eV, 5.32 eV and 5.41 eV, respectively, which are in good agreement with those estimated by LeBreton et al. [44]. Interestingly, the IPs of the solvated systems has the same order $G < A < C < T$ as found in gas-phase [33–43] (Table 20-1).

In double stranded DNA, base pairs (shown in Figure 20-2) represent the fundamental units and their IPs have been studied in detail in a series of investigations. The base pair donor hydrogen bonds provide increased stability for the cation radicals formed and also provide opportunities for interbase proton transfer. In Table 20-2, we present the adiabatic and vertical IPs of GC and AT base pairs calculated using a variety of methods. Using Koopmans' theorem, Colson et al. [46] estimated the IPs of DNA bases in the AT and GC base pairs at HF/3-21G and HF/6-31+G(d)//HF/3-21G levels of theory. They found that the IPs of A and T in AT base pair was unaffected while the IPs of G and C in the GC base pair was modified significantly and IP of G was lowered by 0.54 eV and IP of C was increased by 0.58 eV. This is easily understood as follows. Donor hydrogen bonds stabilize the base cation radical while acceptor hydrogen bonds tend to destabilize the system energetically. In GC the G cation radical has two donor hydrogen bonds and one hydrogen bond acceptor while in AT the A cation radical has one donor

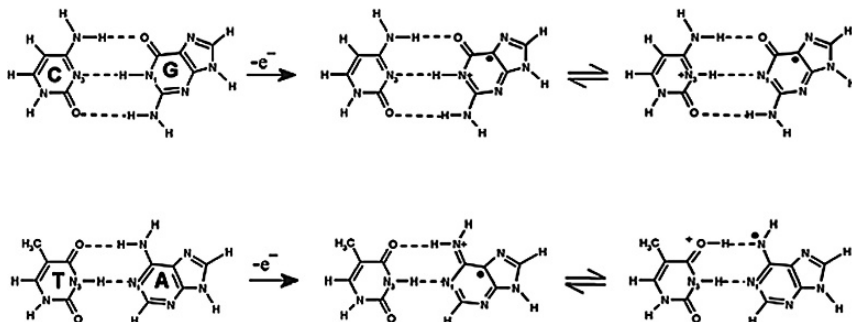


Figure 20-2. Scheme showing the neutral, one electron oxidized and proton transfer reactions in GC and AT base pairs in DNA

and one acceptor H-bond (see Figure 20-2). Using the B3LYP/6-31+G(d) method, Li et al. [47] calculated the adiabatic and vertical ionization potentials of GC and AT base pairs. The zero point energy (ZPE) corrected IPs of GC and AT base pairs are found to be 6.90 and 7.68 eV, respectively. Hutter and Clark [48] also calculated the adiabatic IPs of GC and AT base pairs and after a linear correlation to experimental IP values they estimated 7.08 and 7.79 eV for GC and AT base pairs, respectively. However, Bertran et al. [49] estimated adiabatic IP of GC and AT base pairs as 6.96 and 7.79 eV, respectively. These results predict that GC base pair has the lowest IP in comparison to the AT base pair. These theoretical results show that GC base pair in DNA is the preferred site for hole stabilization with the hole localize on G. Li et al. [47] further calculated the reorganization energy for an adiabatic electron transfer (ET) process in which a hole begins on a base pair and ends on the base pair of the same type. They calculated the reorganization energies of AT and GC base pairs as 0.37 eV and 0.70 eV, respectively, which are the sum of the two relaxation energies, i.e., the nuclear relaxation energy after hole formation in a base pair and the relaxation energy after recombination of the electron and the relaxed base pair cation [47]. This suggests that hole transfers through stacked AT base pairs more rapidly because of the low reorganization barrier. This is in agreement with results found in experiments of Giese et al. [50], Sartor et al. [51] and recently by Majima et al. [52].

While these studies give good estimates for the IPs, it has been shown that the properties of DNA components are affected by the first few waters of hydration which mimic the first hydration shell around the molecule. For example, each water that acts as a net hydrogen bond donor to a base results in an elevation of the IP while each water that acts as a net hydrogen bond acceptor will tend to lower the IP [54]. The solvation model, e.g., PCM (polarized continuum model), which takes into account the effect of the bulk solvent on the solute lacks these specific interactions and has the effect of substantially lowering the IP. Nevertheless, these first waters need to be included for a good accounting of IPs and EAs.

Table 20-2. Ionization potential (IP) of GC and AT base pairs in gas-phase and in hydrated system

Method	GC		AT		GC+4H ₂ O		AT+4H ₂ O	
	IP _{adia}	IP _{vert}	IP _{adia}	IP _{vert}	IP _{adia}	IP _{vert}	IP _{adia}	IP _{vert}
HF/3-21G ^a	6.13	7.46 ^b	7.14	8.36 ^b		7.80 ^f		8.59 ^f
HF/6-31+G(d) ^{a,c}	6.24	7.71 ^b	7.08	8.42 ^b	6.53 ^g		7.45 ^g	
B3LYP/6-31+G(d)	6.90 ^d	7.23	7.68 ^d	7.80				
B3LYP/D95*/UHF/6-31G*	6.71(7.08) ^e		7.45(7.79) ^e					

^aRef. [46]; ^bKoopmans' IP is taken as the energy of the highest occupied molecular orbital (HOMO) and is a good estimate of the vertical IP; ^cGeometries were optimized by HF/3-21G method; ^dZero point energy (ZPE) corrected value [47]; ^eValues obtained from a linear correlation to experimental IP values for single bases; ^fKoopmans' approximation [53]; ^gRef. [54].

In early work, Colson et al. [53, 54] calculated the ionization potentials of GC and AT base pairs surrounded by four water molecules. In the study, they used HF/3-21G* and HF/6-31+G(d)//HF/3-21G* methods. Using Koopmans' theorem, they calculated the vertical ionization potential (IP_{vert}) of GC and AT base pairs to be 7.80 and 8.59 eV, respectively (Table 20-2). However, the corresponding adiabatic ionization potential (IP_{adia}) calculated using HF/6-31+G(d)//HF/3-21G* method was found to be 6.53 and 7.45 eV, respectively. These values are larger than found without water as a result of most of the waters acting as H-bond donors. These values however did not consider bulk solvation on the DNA structure and this has been considered more recently by Schuster et al. [55] who studied the neutral and cationic form of duplex DNA $d(5'-(G)_n-3')$, for $n = 2$ and $n = 3$ with the base pairs arranged in the standard crystallographic structure. In the calculation, the phosphate group was neutralized by Na^+ counterions and structure was solvated by water molecules. They calculated the vertical IP [$d(5'-(G)_3-3')$] = 4.67 eV and vertical IP [$d(5'-(G)_2-3')$] = 5.94 eV. The adiabatic IP of $d(5'-(G)_2-3')$ was calculated to be 5.44 eV. Using HF and MP2 methods and cc-pVDZ basis set, Hutter [56] recently reported the IP of GGG in the range of 5.64–7.07 eV, respectively. The ionization potentials of stacked DNA base guanine are also calculated by Prat et al. [57] and Sugiyama and Saito [58]. These results show that in DNA the site which has several stacked guanine bases corresponds to the preferred site for oxidation or has lowest ionization potential [56–58].

20.2.2. Proton Transfer Reactions in Base Pair Ion Radicals

Experimental work [59–64] has shown that proton transfer between bases in base pairs can further stabilize a base pair ion radical (see Figure 20-2). Such proton-transfer reactions have been shown to regulate hole and electron transfer processes through the stacked DNA bases. Steenken [59, 60] first considered those proton transfer reactions in base pair ion radicals where hydrogen bonded protons likely transfer between base pairs. He [59, 60] also noted that acidity of the complementary purine base and the basicity of the radical anion would affect the extent of such a proton transfer. For example, the pK_a of deoxyguanosine is 9.4 (weak acid) and pK_a of cytosine radical anion ($C(N3H)^\bullet$) is ≥ 13.0 (strong base), thus a proton transfer from guanine to cytosine radical anion is favored. However, the pK_a of deoxyadenosine is ≥ 14 (very weak acid) and pK_a of $T^{\bullet-}$ ($T(O4H)^\bullet$) is ≥ 6.9 (weak base) and thus proton transfer from A to $T^{\bullet-}$ is very unlikely. Similar reasoning to the one electron oxidized GC and AT base pairs was also applied [59, 60].

For comparison to these predictions from experimental results [59, 60], Colson et al. [46, 65] studied the proton transfer reactions in GC and AT base pairs in their radical cationic and anionic states using HF/3-21G* and HF/6-31+G(d)//3-21G* levels of theory (see Figure 20-2). Their calculated proton transfer energies (difference between the total energies of the ionized radical base pairs before and after proton transfer) at HF/3-21G* level of theory correlated very well with

the experimental values determined by Steenken [59, 60]. Theoretical calculations [46] are also able to predict the similar tendencies for proton transfer as shown in Table 20-3. More recently, the proton transfer reaction in radical ions of GC and hypoxanthine-cytosine base pairs has been investigated in detail by Li et al. [47b] at B3LYP/6-31+G(d) level of theory. They calculated the activation barrier (transition state) for the interbase proton transfer, and the corresponding enthalpy (ΔH) and the free energy (ΔG). It was also concluded from the thermodynamic data (activation barrier, ΔH and ΔG) that proton transfer is predicted to be highly favored in the GC anion radical base pair while it is less favorable for GC cation radical [47b]. These GC anion radical results are in excellent agreement with predictions from experiment (Table 20-3) whereas those for the GC cation radical are in slight disagreement ca. 2 kcal/mol. From vibrational analyses Li et al. [47b] also concluded that oscillatory motion in DNA can promote proton transfer as proposed for the phonon assisted proton-electron transfer process along the DNA [66]. The proton-coupled charge/electron-transfer mechanism received wide attention from experimental and theoretical point of views [60, 67–71]. In this scenario, the charge hopping is linked to the proton transfer from G to C. Hutter and Clark [48] and Bertran et al. [49] earlier calculated the proton transfer reaction in radical cations of GC and AT base pairs. Bertran et al. [49], using B3LYP/6-31G** method, found that both $GC^{\bullet+}$ and $AT^{\bullet+}$ and the corresponding proton transferred complexes (Table 20-3) have almost identical ΔG s (ca. 1.3 kcal/mol). Hutter and Clark [48] using UB3LYP/D95**/UHF/6-31G* level of theory, found that $GC^{\bullet+}$ and its proton transferred analog ($^{\bullet}G(-H1^+)C(+H3^+)^+$) after ZPE correction differ by 1.6 kcal/mol. Not surprisingly from these theoretical results, Nir et al. [72] observed a fast $G \rightarrow C$ proton transfer on a nanosecond time scale using resonance-enhanced multiphoton ionization (REMPI). From Table 20-3, except for those for $AT^{\bullet+}$ we see that all the theoretical methods agree well suggesting even the lowest theoretical level employed gave quite predictive results. For $AT^{\bullet+}$ it is interesting that the

Table 20-3. Calculated proton transfer energies (kcal/mol) along with experimental values

Proton transfer reaction ^a	ΔE (ΔG)			Expt ^b	
	HF/3-21G* ^c	B3LYP/6-31+G(d) ^d	B3LYP/6-31G** ^e	pK _a	ΔG
$GC^{\bullet+} \rightarrow ^{\bullet}G(-H1^+)C(+H3^+)^+$	1.18	1.25 (1.39)	1.4 (1.3) {1.6} ^f	-0.5	-0.7
$GC^{\bullet-} \rightarrow ^{\bullet}C(+H3^+)G(-H1^+)^-$	-4.91	-3.16(-3.11)		≥ -3.5	≥ -4.8
$AT^{\bullet+} \rightarrow ^{\bullet}A(-H10^+)T(+H9^+)^+$	-1.94		1.5 (1.4)	≥ 6.0	≥ 8.2
$AT^{\bullet-} \rightarrow ^{\bullet}T(+H9^+)A(-H10^+)^-$	4.85			≤ 6.85	≤ 9.3

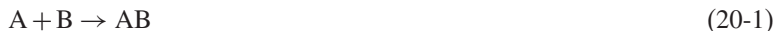
^aSee Figure 20-2; ^bDetermined from equilibrium constants estimated by Steenken (ref. [59]); ^cRef. [46];

^dFree energy (ΔG). Zero point energy (ZPE) corrected free energy (ΔG), calculated at 298 K in kcal/mol, is given in parenthesis (ref.[47b]); ^eRef. [49]; ^fHutter and Clark [48]. ZPE corrected ΔE calculated using UB3LYP/D95**/UHF/6-31G* method.

experiment suggests no transfer but theory predicts transfer. This point has not been tested in experimental work to date.

20.2.3. Base Pairing or Interaction Energies

The base pairing or interaction energy (ΔE) is defined as the difference between the total energy of the base pair and the sum of the total energies of the isolated bases. In base pairs it is also defined as hydrogen bonding energy. If we consider the following reaction



where, A and B are two interacting bases (reactants) to form base pair AB (product). The enthalpy of the reaction at a given temperature 298.15 K and 1 atm (ΔH_{298}) is calculated from 0 K electronic bond energy (ΔE_{elec}), assuming an ideal gas [73], is given as follows

$$\Delta H_{298} = \Delta E_{\text{elec}} + \Delta E_{\text{trans},298} + \Delta E_{\text{rot},298} + \Delta E_{\text{vib},0} + \Delta(\Delta E_{\text{vib}})_{298} + \Delta(pV) \quad (20-2)$$

Here, $\Delta E_{\text{trans},298}$, $\Delta E_{\text{rot},298}$ and $\Delta E_{\text{vib},0}$ are the differences between products and reactants in translational, rotational and zero point vibrational energy, respectively. $\Delta(\Delta E_{\text{vib}})_{298}$ is the change in the vibrational energy difference as one goes from 0 to 298.15 K. $\Delta(pV)$ is the molar work term, $(\Delta n)RT$ and $\Delta n = -1$ for two components combining to one molecule.

In Table 20-4, we present theoretically calculated pairing energies along with experimentally determined values due to Yanson et al. [74] using mass spectrometry data. Colson et al. [46], using HF/3-21G and HF/6-31+G(d) methods, calculated the pairing energies of GC and AT base pairs in their neutral, radical anionic and cationic states. The base pairing energies calculated at HF/6-31+G(d) level, -23.02 and -10.03 kcal/mol, of neutral GC and AT base pairs are slightly lower (~ 3 kcal/mol) than the experimental values [74], after ZPE correction the corresponding values are -21.13 and -8.65 kcal/mol, respectively. Almost similar values were obtained using B3LYP/6-31+G(d) method by Li et al. [47a], Table 20-4, (BSSE corrections were not done and such corrections would reduce these values ca. 1–2 kcal/mole). We noticed that neutral base pairs have been extensively studied and we do not attempt to fully review this literature. A good deal of earlier work on neutral base pairs may be found in references [75] and [76]. Using advanced level of theory the interaction energy of neutral AT and GC base pairs in Watson-Crick as well as in other conformations has been calculated recently [75, 76] and are presented in Table 20-4 for comparison purposes. Several of these values for the GC base pair are substantially overestimates (> 12 kcal/mol) the experimental value [74]. On the other hand, HF and DFT methods [46, 47a, 49, 75–78] using compact basis sets

Table 20-4. Base pairing/interaction energy of GC and AT base pairs in their neutral, anionic and cationic radical states

Method	Refs.	Pairing/interaction energy (ΔE)		
		G + C \rightarrow GC	G ^{•+} + C \rightarrow G ^{•+} C	G + C ^{•-} \rightarrow GC ^{•-}
HF/6-31+G(d)	46	-23.02	-38.05	-34.99
B3LYP/6-31+G(d) ^a	47a	-22.9 (23.5)	-40.5 (-41.1)	-36.2 (-36.78)
B3LYP/6-31G ^{*ab}	49	-24.0	-43.0	
UHF/6-31G ^{sf}	48	-27.5		
B3LYP/6-31G(d,p) ^b	77	-25.0	-40.9	
MP2 ^c	75	-31.6		
CCSD(T) ^c	75	-32.1		
DFT-SAPT ^d	76	-30.5		
Exp ^e	74	-21.0		
		A + T \rightarrow AT	A ^{•+} + T \rightarrow A ^{•+} T	A + T ^{•-} \rightarrow AT ^{•-}
HF/6-31+G(d)	46	-10.03	-17.05	-8.79
B3LYP/6-31+G(d)	47a	-10.7 (11.3)	-20.6 (-21.2)	-12.85 (-13.44)
B3LYP/6-31G ^{*ab}	49	-10.9	-21.7	
UHF/6-31G ^{sf}	48	-12.3		
B3LYP/6-31G(d,p) ^b	78	-12.0	-22.9	
MP2 ^c	75	-16.9		
CCSD(T) ^c	75	-16.9		
DFT-SAPT ^d	76	-15.7		
Exp ^e	74	-13.0		

^aZPE corrected values. In parentheses, ZPE corrected enthalpy (ΔH) are calculated at 298.15 and 1.0 atm; ^bBasis set superposition error (BSSE) corrected values; ^cCalculated using complete basis set (CBS) limit; ^dDensity functional theory (DFT) including symmetry-adapted perturbation theory (SAPT); ^eTemperature-dependent field ionization mass spectroscopic measurements; ^fZPE corrected values.

predict quite reasonable values (see Table 20-4). Although the physical properties of the neutral base pairs have been studied extensively, the studies of base pairs in their ionized states are far fewer in number. From Table 20-4, with the exception of AT^{•-}, it is clear that base pair ion radicals are stronger than neutral base pairs. The pairing energies of GC^{•+}, GC^{•-} and AT^{•+} are predicted to be almost two times stronger than in the neutral base pair by all the theoretical methods [46, 47a, 49, 77, 78]. As seen from the Table 20-4, the pairing energy in AT^{•-} is similar to the corresponding neutral system. The reason for lack of increase in the value on base pairing in AT^{•-} likely lies in the site of the localization of the excess electron and unpaired spin density at C6 on thymine away from the hydrogen bonding sites. In the cases of GC and AT cation radicals the hydrogen bonds are greatly polarized by the radical formation increasing the hydrogen bond energies.

20.2.4. Gas Phase Electron Affinities of DNA Bases and Base pairs (Valence and Diffuse States)

It is well understood that all of the DNA components, bases, sugar, phosphates have gas phase vertical electron affinities (VEAs) that are negative in value. Only in aqueous systems do the most electron affinic of the DNA components, the DNA bases, have large enough electron affinities to readily trap excess electrons and form stable anion radicals. While in the gas phase the vertical electron affinities of all the DNA bases are negative (Table 20-5), the adiabatic electron affinities of the DNA bases are near zero for T, U, and C but negative for A and G [7, 79–88]. The terms used in this section for various electron attachment detachment energies, VEA, AEA and VDE, are defined in Figure 20-3. Recently, several reviews have been appeared that deal with the electron affinities of the DNA bases [7, 79, 80]. The review by Svozil et al. [79] gives an excellent overview of this area. In Table 20-5, we present a summary of our opinion of the best estimates for the vertical and adiabatic valence EAs from experiment and theory. In Table 20-6, we show a detailed listing of the calculated and the experimental values. Recently, Vera and Pierini [82] have used standard DFT methods and compared DFT results with experimentally measured values of the vertical valence electron affinities of 30 compounds with good results (± 0.2 eV). However, we note that the DFT calculated values for the AEAs are likely more positive than experiment by ca. 0.15 eV [87]. This is an inherent problem with the DFT functionals and is not found for high level ab initio HF calculations such as CCSD(T) or CBS-Q (Table 20-5).

In Tables 20-5 and 20-6, we see that the largest disagreement among calculated values is for the base guanine, which has theoretical AEA values from -0.7 to 0 eV. The values near zero are a result of basis sets with diffuse functions which mix valence states with diffuse “dipole bound” states and do not represent good

Table 20-5. Best estimates of valence electron affinities (eV)

Type	Vertical		Adiabatic		ab initio ^{ref}
	Exp ^a	Theory	Exp	Theory	
Refs.	94	87 ^b , 35,82 ^c	95 ^d	87 DFT ^e	
G	-0.74^f	-1.25		-0.75	-0.52^{96}
A	-0.54	-0.74		-0.35	
C	-0.32	-0.55		-0.05	-0.13^{88}
T	-0.29	-0.30	Ca.0	0.15	0.02^{97}
U	-0.22	-0.27	Ca.0	0.20	0.002^{88}

^aElectron transmission spectroscopy results; ^bB3LYP/D95V+(D) except for G which is estimated from trends; ^cDFT (B3LYP/6-311+G(2df,p)); ^destimated from stable valence anion complexes, e.g., U(Ar)⁻; ^ebest estimates from DFT basis set dependence study (vide infra). Thymine from ref. [88], note these values are likely too positive by 0.15 eV; ^fEstimate of keto tautomer from enol tautomer experimental value (-0.46 eV) plus calculated difference in energy between keto and enol tautomers (0.28 eV) ref. [94].

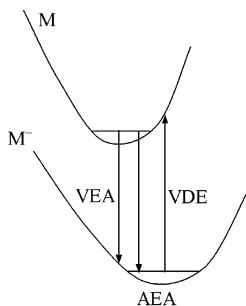


Figure 20-3. Electron binding energies for molecule M in anionic state are defined pictorially in a representation of the potential energy surfaces of the neutral molecule (M) and anion radical (M^-) with the lowest vibration energy level shown for each. During a vertical process, the geometry remains unchanged but for the adiabatic process structural relaxation occurs. Thus the VDE (vertical detachment energy) and VEA (vertical electron affinity) represent the upper and lower bounds to the adiabatic electron affinity (AEA)

estimates of the valence EA. The mixing of diffuse states and valence states is a major difficulty in obtaining accurate valence electron affinities theoretically and is not limited to guanine but includes all molecules having near zero or negative electron affinities [82–84]. Only stable bound states are readily accessible to DFT or HF theories, and for molecules with negative valence electron affinities, no stable bound state exists, other than dipole-bound or continuum states. Nevertheless, experiments employing electron transmission spectroscopy (ETS) [82, 85, 86] are able to experimentally measure negative electron affinities, i.e., those molecular states that exist above the zero of energy in the continuum [87, 88]. Since negative electron affinities are experimentally available, a number of “practical” methods, for dealing with negative electron affinities theoretically, have been proposed and used in the literature [87, 88]. The chief one is the use of small basis sets that confine the electron to the molecular framework and produce reasonable estimates of the relative valence electron affinities with absolute values estimated by interpolative techniques [86, 89, 90]. Along these lines, Li et al. [87] performed a series of DFT (B3LYP functional) calculations using basis sets of differing size. The trends with basis set, along with the SOMO (singly occupied molecular orbital), clearly show when the diffuse states mix with valence states. The resulting best values for adiabatic and vertical electron affinities are summarized in Table 20-5. We note that in solution diffuse states are energetically unfavorable while compact ion (valence) states are stabilized by the bulk dielectric by several eVs so that in aqueous media all DNA base anions have been observed experimentally by electron spin resonance (ESR) as valence anion radicals [91–93].

While adiabatic EAs of U and T are known from experiment to be 0 ± 0.1 eV, the uncertainty in the values for the purines A and G is much greater. A and G clearly have negative adiabatic electron affinities which DFT theory suggests to be ca. -0.35 eV (A) and -0.5 to -0.75 eV (G) with their vertical electron affinities

Table 20-6. Gas phase electron affinities (eV) derived from experiment and theory

Experiment		Theory							
Refs.	VEA	AEA	Method	Refs.	VEA	AEA	Type ^o		
Guanine (G)	94 ^a	-0.46	-	MP2/6-31+G(d) ^b	33	-1.23	-	VB	
				B3LYP/D95V+(D) ^c	87	-1.25	-0.75	VB	
				MP2/aug-cc-pVDZ ⁱ	96	-0.39	-0.63(0.036)	VB(DB)	
				CCSD/ aug-cc-pVDZ ⁱ	96	-	-0.52(0.056)	VB(DB)	
				CCSD(T)/aug-cc-pVDZ ⁱ	96	-	-0.49(0.065)	VB(DB)	
				B3LYP/6-31+G(2df,p) ^d	35,82	-	-0.27	MS	
				B3LYP/DZP++ ^e	89	-	-0.10	MS	
				B3LYP/TZ2P++ ^f	89	-	0.07	MS	
				B3LYP/TZVP ^g	34	-	-0.38	VB-MS	
				B3LYP/6-311++G**g	34	-	0.00	MS	
	Adenine (A)	94 ^a	-0.54	-	MP2/6-31+G(d) ^b	33	-0.74	-0.30	VB
		98 ^h	-0.45	-	B3LYP/D95V+(D) ^c	87	-0.80	-0.35	VB
				B3LYP/6-31+G(2df,p) ^d	35,82	-0.69	-0.40	VB	
				B3LYP/DZP++ ^e	89	-	-0.28	VB	
				B3LYP/TZ2P++ ^f	89	-	-0.17	MS	
				B3LYP/TZVP ^g	34	-	-0.48	VB	
				B3LYP/6-311++G**g	34	-	-0.26	VB	

(continued)

Table 20-6. (continued)

Experiment		Theory					
Refs.	VEA	AEA	Method	Refs.	VEA	AEA	Type ^o
Thymine (T)							
94 ^a	-0.29	-	MP2/6-31+G(d) ^b	33	-0.32	0.30	VB
95 ^d	-	69±7 (DB)	B3LYP/D95V+(D) ^c	87	-0.28	0.22	VB
99 ^j	-	62±8 (DB)	CBS-Q	88	-	-0.06	VB
99 ^k	-	120±120	B3LYP/6-31+G(2df,p) ^d	35,82	-0.30	0.14	VB
			B3LYP/DZP++ ^e	89	-	0.20	VB
			B3LYP/TZ2P++ ^f	89	-	0.16	VB
			B3LYP/TZVP ^g	34	-	0.08	VB
			B3LYP/6-311++G** ^g	34	-	0.18	VB
			MP2/AVDZ ^m	100	-	-0.14	VB
			CCSD/AVDZ ^m	100	-	-0.12	VB
			CCSD(T)/AVDZ ^m	100	-	-0.087(0.053)	V(DB)
			CCSD(T)/aug-cc-pVDZ ⁿ	97	-	0.018 (0.051)	V(DB)
Cytosine (C)							
94 ^a	-0.32	-	MP2/6-31+G(d) ^b	33	-0.40	0.20	VB
98 ^h	0.55	-	B3LYP/D95V+(D) ^c	87	-0.63	-0.05	VB
99 ^j	-	85±8 (DB)	CBS-Q	88	-	-0.13	VB
99 ^k	-	130±120	B3LYP/6-31+G(2df,p) ^d	35,82	-0.49	-0.06	VB
			B3LYP/DZP++ ^e	89	-	0.03	?
			B3LYP/TZ2P++ ^f	89	-	-0.02	?
			B3LYP/TZVP ^g	34	-	-0.12	VB
			B3LYP/6-311++G** ^g	34	-	0.01	?

(continued)

Table 20-6. (continued)

Experiment		Theory				Type ^o	
Refs.	VEA	AEA	Method	Refs.	VEA	AEA	
Uracil (U)							
94 ^a	-0.22	-	MP2/6-31+G(d) ^b	33	-0.19	0.40	VB
95 ⁱ	-	93±7 (DB)	B3LYP/D95V+(D) ^c	87	-0.32	0.20	VB
99 ^j	-	86±8 (DB)	CBS-Q	88	-	0.00	VB
99 ^k	-	150±120	B3LYP/6-31+G(2df,p) ^d	35,82	-0.26	0.18	VB
			B3LYP/DZP++ ^e	89	-	0.15	VB
			B3LYP/TZVP ^g	89	-	0.19	VB
			B3LYP/TZVP ^g	34	-	0.14	VB
			B3LYP/6-311++G** ^g	34	-	0.22	VB

^a From low-energy electron transmission spectroscopy (LETS). The VEA for guanine enol tautomer; ^b Scaled ab initio HF at MP2/6-31+G(d); ^c Best estimate from ref. [87]; ^d Single point calculation. Geometries were optimized using B3LYP/6-31+G(d,p); ^e Zero point energy (ZPE) corrected values; ^f Single point calculation. Geometries were optimized using B3LYP/DZP++; ^g Zero point energy (ZPE) corrected values; ^h Rydberg electron spectroscopy (RETS). Values are in eV; ⁱ Values are in meV. Dipole bound excess electrons; ^j Photodetachment-photoelectron (PD-PE) spectra. Dipole bound excess electron. Values are in meV; ^k PD-PE spectra. Estimated from experiment by extrapolation of data for hydrated bases. Valence bound excess electrons. Values are in meV; ^l Valence bound AEA. In parentheses, dipole bound AEA is given; ^m Valence bound AEA. In parentheses, dipole bound AEA is given; ⁿ Valence bound AEA. In parentheses, dipole bound AEA is given. The valence state AEA is obtained after ZPE correction and higher order CCSD(T) correlation corrections to the MP2 complete basis set (CBS) limit. For details see ref. [97]; ^o V, DB and MS refer to valence bound, dipole bound and mixed state, respectively.

more negative, i.e., -0.74 eV (A) [82, 87] and -1.25 eV (G) [82, 87]. Experiment suggests these theoretical vertical values are somewhat too low. However, both theory and experiment agree that the vertical EA for G and A are so negative that nuclear relaxation will not raise the adiabatic EAs to positive values. Of course, these virtual states (i.e. negative electron affinities) for A and G in the gas phase become more relevant to biology when they become bound states in solvated systems.

The zero-point energy difference (ZPE) between the neutral and its anion is a good indicator of the degree of molecule-electron interaction. The zero-point vibrational energy is affected by the excess electron to the extent that the electron causes reorganization in the molecular framework. In the extreme case that the electron is lost in the continuum, there will be no change in the ZPE contribution before and after the addition of the electron. Thus, these calculations clearly show at what basis set size (especially number of diffuse functions) the valence state becomes contaminated with significant contributions from diffuse states. In Table 20-7, we see the change with basis set for A and G but no change is found for U, T and C as they maintain valence states for each of the basis sets.

Recently, the radical anions of adenine-thymine (AT) and 9-methyladenine and 1-methylthymine (MAMT) have been studied by Bowen, Gutowski and co-workers using both experiment and theory [101]. From photoelectron spectra (PES) of AT and MAMT radical anions they found that the spectra are very different from one another with vertical detachment energies (VDEs) of 1.7 and 0.7 eV, respectively. Using B3LYP/6-31+G** method, they calculated the VDE of AT radical anion (in Watson-Crick (WC) conformation) as 0.89 eV which is quite different from the experimental value of 1.7 eV [101]. However, using the B3LYP/6-31+G** method, they [101] found a barrier-free proton transfer (BFPT) structure for AT radical anion, which has the VDE comparable to the experimental value. On the other hand, the B3LYP/6-31+G** calculated VDE (0.77 eV) of MAMT anion radical corresponds very well to the experimental value [101] (see Table 20-8). In recent years, electron affinity (EA) of AT and GC base pairs in gas phase have been studied using DFT method [47a, 101–104] and we found that all the theoretical calculations [47a, 101–104] predicted the AEA of AT in the range 0.30–0.36 eV, respectively, while AEA of GC base pair lies in the range 0.49–0.60 eV, respectively,

Table 20-7. Zero point energy differences (ZPE) [ZPE neutral – ZPE anion] (eV)

Basis set ^a	U	T	C	A	G
6-31G(D)	0.17	0.17	0.10	0.20	0.27
D95V(D)	0.16	0.16	0.09	0.19	0.26
6-31+G(D)	0.17	0.16	0.10	0.12	0.06
D95V+(D)	0.17	0.16	0.09	0.12	0.06
6-311++G(2d,p)	0.17	0.17	0.10	0.03	0.04

^a See ref. [87]

Table 20-8. Gas phase electron affinities (eV) of AT and GC base pairs derived from experiment and different theoretical methods

AT base pair					
Experiment		Theory			
Ref	VDE	Method	Ref	AEA	VDE
101	0.7 ^a	B3LYP/6-31+G(d)	47a	0.30 ^b	0.60
		B3LYP/DZP++	102	0.36 ^b	–
		B3LYP/DZP++ ^c	103	0.60 ^b	1.14
		B3LYP/6-31+G** ^d	101	–	0.89
		B3LYP/6-31+G** ^e	101	–	0.77
		SCC-DFTB-D ^f	104	0.36	–
GC base pair					
		B3LYP/6-31+G(d)	47a	0.49 ^b	1.16
		B3LYP/DZP++	105	0.60 ^b	–
		SCC-DFTB-D ^f	104	0.56	–

^a Photoelectron spectroscopy (PES) of 9-methyladenine and 1-methylthymine (MAMT) radical anion base pair. For AT radical anion the VDE (1.7 eV), from PES, was considered as the barrier free proton transfer species [101], and does not correspond to the WC conformation; ^b Zero point energy corrected values; ^c Nucleoside pair, Deoxyriboadenosine (dA)-Deoxyribothymidine (dT); ^d AT base pair anion in Watson-Crick (WC) conformation; ^e 9-methyladenine-1-methylthymine (MAMT) anion; ^f Self-consistent charge, density functional tight binding (SCC-DFTB-D) method.

see Table 20-8. The B3LYP/6-31+G(d) calculated VDE of AT base pair from the work of Li et al. [47a] is in close agreement with experimental VDE of MAMT [101]. In Table 20-8, we compared the theoretical VDE values of AT base pair with experimental VDE of MAMT [101] because this corresponds to the Watson-Crick (WC) conformation as considered in all the theoretical studies [47a,101–104].

20.2.5. Effect of Solvation on the Electron Affinity (EA) of Bases and Base Pairs

Solvation of DNA bases/base pairs is of fundamental importance to biological processes as they take place in aqueous media. The effect of hydration on neutral bases or base pairs has been addressed using quantum chemical methods [106–112] as well as molecular dynamics (MD) simulations [113, 114]. It is known that unlike the gas phase, dipole bound anions do not exist in condensed environments because such diffuse states are destabilized in the aqueous phase [115]. The drastic change in the nature of excess electron binding in the presence of water molecules with uracil has been observed experimentally by Bowen and co-workers [95b] using negative electron photoelectron spectroscopy (PES). They observed that even with a single water molecule the dipole bound state of uracil anion in gas phase

completely transferred to the covalent bound uracil anion [95b]. Subsequently, this was also confirmed by Periquet et al. [98] using Rydberg electron transfer spectroscopy (RETS) and Schiedt et al. [99] using photodetachment-photoelectron (PD-PE) spectroscopy. Further, Schiedt et al. [99] observed that electron affinities of solvated uracil, thymine and cytosine increases linearly with the number of hydrating water molecules. They [99] used these values to extrapolate back to the bare DNA base and reported AEAs for T, C and U of ca. 0.1–0.15 eV (Table 20-6); however these values are likely overestimated by ca. 0.1 eV because the assumption of linearity does not properly account for the fact that the first water of hydration has a significantly larger hydration stabilization to the AEA than subsequent waters of hydration.

Of course, it is clear that the incorporation of solvent effect on the electron affinities of the DNA bases or base pair is crucial in understanding the DNA damage in biological relevance. Using theoretical tools, the solvation of a molecule can be modeled as follows: (i) considering the bulk solvent such as polarized continuum model (PCM) and (ii) placing a number of water molecules surrounding the molecule in question. While PCM model appropriately represents the bulk solvent, it cannot explicitly take into account the hydrogen bonding between solute and solvent. On the other hand, the water molecules, surrounding the molecule, while they provide the information about the solute-solvent interaction (hydrogen bonding) and computationally very expensive and miss the full effect of the bulk dielectric. In recent years, a number of studies appeared in the literature regarding the structure and electron affinities of DNA bases and base pairs including the effect of bulk solvent or hydration [87, 106, 116–125].

Colson et al. [54], in their early work, investigated the effects of hydration of base pairs on the adiabatic electron affinities (AEAs) of thymine and cytosine in the presence of three and four water molecules at the HF/3-21G and HF/6-31+G(d)//HF/3-21G level of theories. Using additive correction constants, they obtained positive AEAs for hydrated base pairs and also predicted positive AEA for both thymine and cytosine bases [54]. By solvating the hydrated (3 and 4 waters) base pairs in the bulk water as solvent ($\epsilon = 78$), the corresponding AEAs [54] increased substantially and lie in the range 0.8–1.3 eV, respectively. Recently, Li et al. [87] calculated the AEAs of G, C, A, T and uracil (U) using the polarized continuum model (PCM) at the B3LYP/D95V+(D) level of theory. The calculated adiabatic electron affinities (AEAs) of U, T, C, A, and G were found to be in the range 1.01–2.14 eV, respectively, see Table 20-9. Frigato et al. [116] calculated the EAs of thymine complexes with one water in their valence and dipole bound states. For valence bound state, they used MP2/6-31G* method while aug-cc-pVDZ basis set with additional set composed of very diffuse functions was used for the dipole bound state [116]. The calculated AEAs [116] of valence bound (VB) anions lie in the range of 0.066–0.29 eV, while dipole bound (DB) anions lie in the range 0.004–0.060 eV, respectively. In a recent work, Schaefer and co-workers [117–121] calculated the EAs of thymine (T), uracil (U), and cytosine (C) in the presence of 1–5 waters using B3LYP/DZP++ method. For U+5H₂O, T+5H₂O, and C+5H₂O

Table 20-9. Adiabatic electron affinities (AEAs) of T, C, U, G and AT base pair in solution using different methods and basis set

Thymine (T)					
Method	Ref	AEA (eV)		VDE (eV)	
		PCM	No. of waters (n) ^a	PCM	Water
HF/6-31+G(d)	54	–	1.3 ^b (4)	–	–
B3LYP/D95+(D) ^c	87	2.06	–	–	–
MP2/CBS+ ΔE_{cc}^d	116	–	0.07–0.29 (1)	–	0.70–0.98
B3LYP/DZP++ ^c	118	–	0.59–0.91 (5)	–	1.28–1.60
B3LYP/6-31++G**	100	1.85	–	2.98	–
Cytosine (C)					
HF/6-31+G(d)	54	–	1.1(3) ^b	–	–
B3LYP/D95+(D) ^c	87	1.89	–	–	–
B3LYP/DZP++ ^c	119	–	0.28–0.61 (5)	–	0.41–1.65
Uracil (U)					
B3LYP/D95+(D) ^c	87	2.14	–	–	–
B3LYP/DZP++ ^c	117	–	0.64–0.96 (5)	–	1.37–1.75
B3LYP/6-31++G**	100	1.94	–	3.10	–
Guanine (G)					
B3LYP/D95+(D) ^c	87	1.01	–	–	–
CCSD(T)/aug-cc-pVDZ	122	1.33	–	3.38 ^f	–
B3LYP/6-311+G**	96	1.41	–	2.65	–
AT base pair					
B3LYP/DZP++ ^g	121	2.05	–	2.51	–
B3LYP/6-31+G** ^h	106	–	0.97 (13)	–	–

^a Number of water molecules in parentheses; ^b Solvated using Onsager reaction field model ($\epsilon = 78$);

^c Single point calculation. Structures optimized using B3LYP/D95V(D) method; ^d For calculation of ΔE_{cc} see ref. [116]; ^e Zero point corrected values. AEAs and VDEs depend on the location of the water molecules, see refs. [117–119]; ^f $\epsilon = 78$ and 2 for the initial and final states, respectively, see ref. [122]; ^g 2'-deoxythymidine-5'-monophosphate-adenine (5'-dTMPH-A) in Watson-Crick (WC) pair;

^h ZPE-corrected AEA.

complexes they calculated the ZPE-corrected AEAs as 0.96, 0.91, and 0.61 eV, respectively. They, also, found that AEAs of T and U increase with the number of hydrating molecules [117–118] in consistent with the experimental observation [99]. Gutowski et al. [100, 122] studied the anions of guanine and thymine in various tautomeric forms using CCSD(T)/aug-cc-pVDZ and B3LYP/6-31++G** methods incorporating PCM model. They found that AEAs of different tautomers of guanine in solution lie in the range 1.33–2.21 eV [122]. Using B3LYP/6-31++G** and PCM model [100] the AEAs of thymine tautomers lie in the range –0.31–1.95 eV,

however, the AEAs of uracil tautomers lie in the range -0.29 – 1.99 eV, respectively. Recently, Kumar et al. [106] studied the neutral and anionic AT base pair in the presence of 5 and 13 water molecules at B3LYP/6-31+G** level. The zero point energy (ZPE) corrected AEA of AT base pair was found to be positive and has the value 0.97 eV [106]. Also, the natural population analysis (NPA) performed using B3LYP/6-31+G** method shows that in the hydrated anionic radical AT complex, the thymine (T) moiety has most of the excess electronic charge, i.e., ~ -0.9 [106].

20.2.6. Dissociative Reactions Due to Low Energy Electron (LEE) Attachment

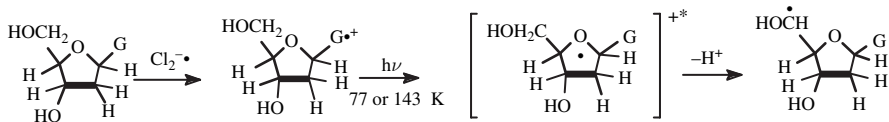
Interaction of LEEs with DNA or DNA bases leads, via dissociative electron attachment (DEA), to hydrogen atom loss and other bond fragmentations [126–134]. Initially, electron attached to a neutral molecule results into the formation of a transient negative ion (TNI) that with the appropriately long autodetachment lifetime, decays into anion and neutral fragments [128]. Hydrogen atom loss from thymine and cytosine has been studied experimentally [128, 131, 135]. Abouaf et al. [136, 137] studied the negative ion production in thymine and 5-halouracils (5-BrU, 5-ClU, 5-FU) due to LEE impact and they observed a long lived BrU^- anion as well as fragment ions Br^- and Uyl^- in the electron energy range 0–3 eV. These studies are of particular biological interest because 5-BrU is used as a radiosensitizer after replacement of thymine in DNA and have potential application in radiation therapy [132–134].

Recently, Li et al. [126, 134, 138] investigated the electron induced carbon halogen bond dissociation for halouracils (5-BrU, 5-ClU, 5-FU). The bond dissociation energies, activation barriers, electron affinities were reported for these halouracil anion radicals as well as the adenine-5-halouracil base pair anion radical at the B3LYP/6-31+G(d) level of theory. In their study [134], they observed, the computed potential energy surface (PES) of dehalogenation of halouracils anion radicals along the C-X (Br, Cl, F) reaction coordinate has several low-lying electronic states: a planar π^* , a dissociative planar σ^* and a non-planar π^* -type mixed state that connects the two planar π^* and σ^* states, respectively. The computed activation barrier (at B3LYP/6-31+G(d) level) of dehalogenation of 5-BrU $^-$, 5-ClU $^-$, 5-FU $^-$ were found to be 1.88 kcal/mol, 3.99 kcal/mol and 20.80 kcal/mol respectively. In the case of U, T and C, they extensively studied the nature of PES of the dissociation of hydrogen atom from different sites of the U, T, and C anions ring plane and found that N1-H bonds are far weaker than the C-H bonds [138]. This theoretical prediction [138] is in excellent agreement with experimental observations of Illenberger and co-workers [139]. Recently, Schaefer et al. [140–145] studied the dissociation of hydrogen atom from different sites of the GC base pair and bases using B3LYP/DZP++ method. In this study, they found, the lowest-energy base pair radical has the hydrogen removed from the N9 of guanine [140].

20.3. SUGAR RADICAL FORMATION AND EXCITED STATE STUDY

In addition to DNA base damage discussed above, sugar radicals are also formed in γ -irradiated DNA and account for about 7–15% of trapped radicals at low temperatures [26–29, 91, 146–150]. Sugar radical formation leads to important types of DNA damage; for example, C1' sugar radical is known to result in an abasic site, whereas C3', C4' and C5' sugar radicals result in strand breaks [29, 151, 152]. The formation of sugar radicals through the abstraction of a hydrogen atom from the sugar ring by the hydroxyl radical is well understood [29, 152] and the formation of sugar radicals via the direct ionization of the sugar phosphate backbone followed by rapid deprotonation is a second well known mechanism [4]. Recently, however, another mechanism of direct formation of sugar radicals has been proposed by Sevilla et al. [27–29, 146–149] which entailed excitation of base cation radicals.

The proposal for base cation excited states arose from work with ion beam irradiations in which high concentrations of sugar radicals were formed predominantly along the ion track, where excitations and ionizations are in proximity. To account for the increased amounts of sugar radicals in ion beam irradiated DNA, it was proposed that excited-state cation radicals could be the direct precursors of the neutral sugar radicals [27–29, 146–149]. The proposed hypothesis was tested experimentally using UV-visible photoexcitation of the $G^{\bullet+}$ (guanine radical cation) in DNA and in model systems of deoxyribonucleosides, deoxyribonucleotides and dinucleoside phosphates [29, 149]. High yields of conversion of $G^{\bullet+}$ to sugar radicals were found in DNA (50%) as well as in model systems (80–100%) [29, 149]. The proposed mechanism for sugar radical formation, shown in Scheme 20-1, was that photoexcitation induced hole transfer from the DNA base one-electron-oxidized radical to the sugar ring which is followed by a rapid deprotonation at specific carbon sites on the sugar ring [29, 146–149]. To further test this hypothesis, excited state calculations, using time-dependent density functional theory (TD-DFT) and 6-31G* basis set, was performed on $G^{\bullet+}$ [148] and A(-H) \bullet [149] in deoxyribonucleosides. This TD-DFT study clearly demonstrated that all the electronic transitions in the near-UV-vis range originate from the inner shell (core) molecular orbitals (MOs) and many of these involved hole transfer to the sugar ring [148, 149] confirming the proposed mechanism (Scheme 20-1). The experimental and theoretical study was, further, extended to larger model systems such



Scheme 20-1. Proposed mechanism of sugar radical formation via photo-excitation. (Reprinted with permission from ref.[149], Nucleic Acid Research, © (2005), Oxford University Press.)

as photoexcitation of $G^{\bullet+}$ in dinucleoside phosphate TpdG cation radical [147]. Again high yields ($\sim 85\%$) of deoxyribose sugar radicals at C1' and C3' sites were observed.

The TD-DFT method is well suited for the neutral as well as for the radical cation systems [147–149, 153–161] with computed vertical transition energies comparable to the experimental results [154–161]. Head-Gordon and co-workers [161] calculated the 11 lowest electronic excitation energies of polycyclic aromatic hydrocarbons (PAHs) radical cations using TD-DFT method considering several functionals and 6-31G** basis set and they found that computed transition energies are within 0.3 eV of the experimental data. Recently, several dinucleoside phosphates (TpdG, dGpdG, dApdA, dApdT, TpdA, and dGpdT) in their cationic radical states were studied by us using the TD-B3LYP/6-31G(d) method [147, 153]. The ground state geometries of all the systems in their radical cation states were optimized at the B3LYP/6-31G(d) method, in their base stacked conformation, for details of the geometry optimization criterion see ref. [153]. Further, the effect of solvation surrounding the dinucleoside phosphates was considered using polarized continuum model (PCM) and transition energies were calculated using TD-B3LYP/6-31G(d) method [147, 153]. In this study, we computed 20 lowest electronic transitions and studied the nature of the electronic transition that takes place from the inner shell (core) molecular orbitals (MOs) to the singly occupied molecular orbital (SOMO) of β -spin. Calculations were performed for a series of dinucleoside phosphates radical cations (TpdG $^{\bullet+}$, dGpdG $^{\bullet+}$, dApdA $^{\bullet+}$, dA $^{\bullet+}$ pdT, TpdA $^{\bullet+}$, and dG $^{\bullet+}$ pdT) and it was found that dG $^{\bullet+}$ pdG and dApdA $^{\bullet+}$ have the lowest first transition energies. Interestingly, we also found that the first transition in all the systems involves hole transfer from base to base as a $\pi - \pi^*$ transition. This is in contrast to our earlier excited state studies of deoxyribonucleosides where the first transition shows hole transfer from base to the sugar moiety [148, 149]. The calculations for dinucleosides suggest that hole transfer from base to base take place at longer wavelengths and hole transfer from base to sugar takes place at higher energies or shorter wavelength. In this regard, the wavelength dependence of sugar radical formation from $G^{\bullet+}$ in 2'-deoxyguanosine (dGuo) and in DNA was also studied by Adhikary et al. [148] by varying the photoexcitation wavelength from visible to UV range. They [148] found that in dGuo the sugar radical formation was independent of the wavelength of light while in dsDNA, above 540 nm no sugar radicals were formed. This important observation is clearly supported by the TD-DFT calculations [147, 153]. In Figure 20-4, we present six selected transitions of dG $^{\bullet+}$ pdG, which covers the visible to near-UV range, along with the plots of molecular orbitals that are involved in the transitions. Transitions S_1 , S_2 , and S_3 (shown in Figure 20-4) correspond to the three lowest transitions whereas the other three transitions presented in Figure 20-4 have been chosen because each has a dominant molecular orbital contribution from a single inner MO.

From Figure 20-4, we see that hole and therefore the SOMO in the ground state cation radical is largely localized on the guanine at 5'-site. The first transition S_1 , occurs between the (SOMO - 1) \rightarrow SOMO and has transition energy 0.59 eV and

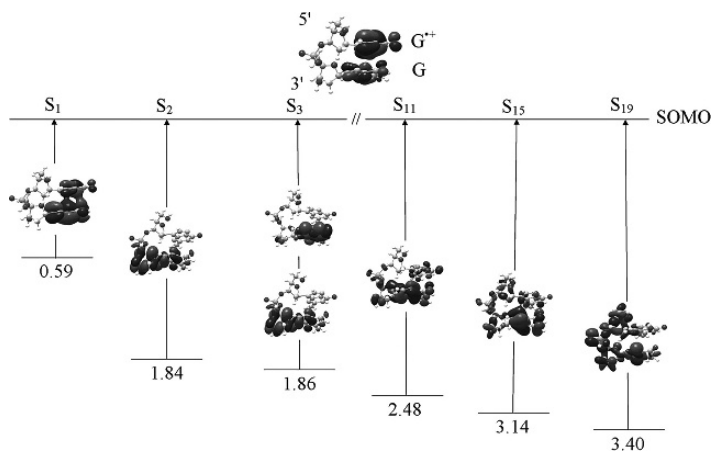


Figure 20-4. TD-B3LYP/6-31G(d) computed transition energies of selected transitions of $dG^{\bullet+}pdG$ cation radical. Excitation energies are given in eV. (Reprinted with permission from ref. [153], *J. Phys. Chem.* © (2006) American Chemical Society.)

has $\pi - \pi^*$ nature. This first transition involves hole transfer from base to base and is clearly depicted in Figure 20-4. However, other transitions involve hole transfer from base to sugar as well as to the phosphate group, in agreement with the experimental findings of sugar radical formation [29, 91, 146–149]. In addition, we were also able to draw several fruitful conclusions from this study. Using CAS-PT2 level of theory, Voityuk et al. [162] recently studied the excitation-induced base-to-base hole transfer in two DNA base in stacked conformations without considering the sugar phosphate backbone. We note that our [153] TD-B3LYP/6-31G(d) computed first transition energies for the dinucleoside phosphates radical cations are in excellent agreement with those computed by Voityuk et al. [162] using CAS-PT2 method (see Table 20-10) except for $dA^{\bullet+}pdA$ and $5'-A^{\bullet+}A-3'$, which differs by 0.4 eV. This discrepancy occurred because CAS-PT2 method gave very small transition energy 0.1 eV for $5'-A^{\bullet+}A-3'$ system [162] due to difficulty in considering the active space in the CASSCF method for this particular system [162]. Recently, Head-Gordon and co-workers [163, 164] pointed out the limitation of TD-DFT method in describing the long-range charge-transfer in excited states. Since in our case, the bases are ~ 3.4 Å apart from each other and base to base electron/hole transfer is operative, thus, it is reasonable to consider this aspect also. A comparison of their approximate approach [163, 164] with TD-DFT [147, 153] (Table 20-10) shows that TD-DFT predicts transition energies quite well for dinucleoside phosphate cation radicals. Further, we note that electrostatic interactions between the bases play an important role in the transition energies. For details of the calculation and nature of the Coulomb interactions between the bases, see ref. [153]. Further, the localization of the hole on the DNA bases is of crucial importance to the charge-transfer process within DNA [18, 58, 165–170]. ESR studies

Table 20-10. Calculated first excitation energies

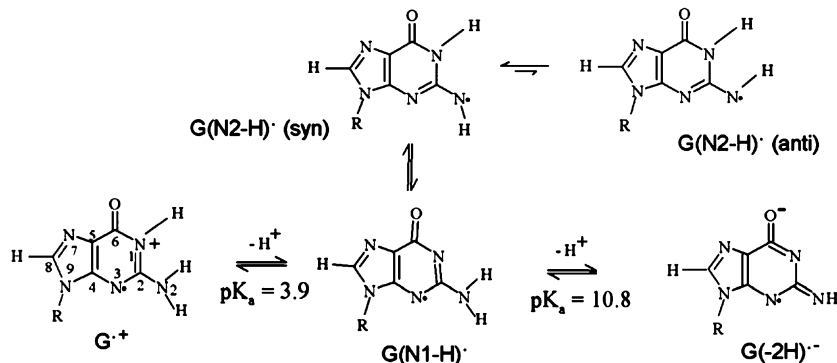
Radical (5'-XY-3')	Method	Excitation energy (eV)	
		Theory (TD-DFT)	Estimated ^b
dG ^{•+} pdG	TD-B3LYP/6-31G(d)	0.59	0.51
G ^{•+} G	CAS-PT2(11,12) ^a	0.39	–
dG ^{•+} pdT	TD-B3LYP/6-31G(d)	1.00	1.06
G ^{•+} T	CAS-PT2(11,12) ^a	1.18	–
TpdG ^{•+}	TD-B3LYP/6-31G(d) ^c	0.76	1.06
TG ^{•+}	CAS-PT2(11,12) ^a	0.80	–
(dApdA) ^{•+}	TD-B3LYP/6-31G(d)	0.52	1.03
A ^{•+} A	CAS-PT2(11,12) ^a	0.10	–
dA(-H) [•] pdA	TD-B3LYP/6-31G(d)	1.43	1.14
dA(-H) [•] pdT	TD-B3LYP/6-31G(d)	1.87	1.73
TpdA(-H) [•]	TD-B3LYP/6-31G(d)	1.80	1.73

^aComplete active space (CAS) ref. [162]; ^bEstimate of first excited-state transition energy as proposed by Head-Gordon and co-workers [163, 164]. For a full description of the details of this calculation see ref. [153]; ^c Ref. [147]. (Reprinted with permission from ref. [153], J. Phys. Chem. © (2006) American Chemical Society.)

clearly show the localization of the hole on a single guanine [32]. From Figure 20-4, we see that SOMO (representing the hole) is mainly localized on the 5'-G (~84% spin density) and a very little (~16 % spin density) is localized on the 3'-G [153]. However, in excited state hole transfers to 3'-G and a little remains on the 5'-G. This result is in complete agreement with earlier studies carried out by Saito and co-workers [58, 167], Hall et al. [168], and Senthilkumar et al. [169], which showed that 5'-G is most easily oxidized in DNA.

20.4. TAUTOMERIZATION IN DEPROTONATED GUANINE CATION RADICAL (G^{•+})

It is well known that DNA radical anions, T^{•-} and C^{•-}, undergo protonation reactions and DNA cation radicals, G^{•+} and A^{•+}, undergo deprotonation reactions [2, 59, 60, 171, 172] as well as water addition reactions [8]. Substantial experimental and theoretical work has been performed on guanine cation radical (G^{•+}) and its deprotonated species but the specific site of deprotonation (N1 or N2 sites) from G^{•+} is still not clear [173–188]. Pulse radiolysis studies [175–177] suggested deprotonation of G^{•+} in 2'-deoxyguanosine (dGuo) from N1 site to give G(N1-H)[•] as shown in Scheme 20-2 but no specific evidence for this site was given. At higher pH, further deprotonation occurs from N2 site of G(N1-H)[•] which gives G(-2H)^{•-} at pK_a = 10.8 [175] (Scheme 20-2). It has also been proposed that in an aqueous environment (water) G(N1-H)[•] would be favored over G(N2-H)[•] [182]. However, using X-ray irradiated single crystals of Guo, dGuo, 5'-dGMP and 3',5'-cyclic



Scheme 20-2. The numbering scheme and prototropic equilibria of one-electron oxidized guanine cation radical ($\text{G}^{\bullet+}$), the mono-deprotonated species, (G(N1-H)^\bullet and G(N2-H)^\bullet , in syn and anti-conformers with respect to the N3 atom) and the di-deprotonated species, $\text{G(-2H)}^{\bullet-}$. (Reprinted with permission from ref. [189], J. Phys. Chem. © (2006) American Chemical Society.)

guanosine monophosphate, ENDOR studies [185–188] shows the production of G(N2-H)^\bullet rather than G(N1-H)^\bullet .

Recently, electron spin resonance (ESR) and theoretical (B3LYP/6-31G(d)) studies have been carried out by Adhikary et al. [189] to identify the preferred site of deprotonation of the guanine cation radical ($\text{G}^{\bullet+}$) in an aqueous medium at 77 K at different pHs. In this work [189], at different pHs, $\text{G}^{\bullet+}$ (pH 3–5), singly deprotonated G(-H)^\bullet (pH 7–9) and doubly deprotonated $\text{G(-2H)}^{\bullet-}$ (pH > 11) were detected. Using the B3LYP/6-31G(d) method, the geometries of all the possible structures (shown in Scheme 20-2) were optimized and their hyperfine coupling constants (HFCCs) were calculated. Singly deprotonated G(-H)^\bullet can exist in three tautomeric forms, i.e., G(N1-H)^\bullet , $\text{G(N2-H)}^\bullet_{\text{syn}}$ and $\text{G(N2-H)}^\bullet_{\text{anti}}$ with conformations defined with respect to N3 atom (Scheme 20-2). The structures of all the three tautomers (G(N1-H)^\bullet , $\text{G(N2-H)}^\bullet_{\text{syn}}$ and $\text{G(N2-H)}^\bullet_{\text{anti}}$) in the presence of a single water molecule, placed near the N1 and NH2 sites of the molecule, were optimized to gain insight about their relative stabilities and to compare with ESR results. The relative stabilities of $\text{G(N1-H)}^\bullet + \text{H}_2\text{O}$, $\text{G(N2-H)}^\bullet_{\text{syn}} + \text{H}_2\text{O}$ and $\text{G(N2-H)}^\bullet_{\text{anti}} + \text{H}_2\text{O}$ are 2.65, 0.00 and 3.63 kcal/mol, respectively. However, on inclusion of bulk solvent as water ($\epsilon = 78.4$) through polarized continuum model (PCM), the relative stabilities of $\text{G(N1-H)}^\bullet + \text{H}_2\text{O}$ and $\text{G(N2-H)}^\bullet_{\text{syn}} + \text{H}_2\text{O}$ were found to be 0.90 and 0.00 kcal/mol, respectively. The relative stabilities of G(N1-H)^\bullet and G(N2-H)^\bullet have been studied, using different theoretical levels, by others [179, 181] and are presented in Table 20-11 along with our calculated values. From Table 20-11, we see that all the studies predict $\text{G(N2-H)}^\bullet_{\text{syn}}$ to be more stable than G(N1-H)^\bullet by 2.7 to 5.0 kcal/mol. These theoretical studies [179, 181, 189], predict the presence of $\text{G(N2-H)}^\bullet_{\text{syn}}$ in the ESR experiment [189] but we found that our calculated B3LYP/6-31G(d) hyperfine coupling constants (HFCCs) did not match very well with our

Table 20-11. Relative stabilities of G(N1-H)[•] and G(N2-H)[•] calculated using different methods and basis sets

Method	Ref	Parent structure	Relative stability (kcal/mol)	
			G(N1-H) [•]	G(N2-H) ^{•a}
B3LYP/6-31G	189	dGuo+H ₂ O (solution) ^b	2.65 (0.90)	0.00, 3.63 anti (0.00)
B3LYP/6-31G	189	dGuo+7 H ₂ O (solution) ^b	0.00 (0.00)	3.26 (3.00)
B3LYP/6-31G ^{*c}	189	9-Met-Gua H ₂ O	2.80	0.00
B3LYP/6-31++G(3df,3pd)//	179	Guanine	4.71	0.00
B3LYP/6-31++G(3df,3pd) ^d		(solution)	(0.00)	(0.91)
B3LYP/6-311G(2pd,p)//6-31G ^{**}	179	Guanine	4.43 ^e	0.00
CPMD ^f	179	Guanine	3.73	0.00
B3LYP/DZP++ ^g	181	Guanine	4.96	0.00, 4.76 anti

^a Unless and otherwise stated G(N2-H)[•] refers to syn conformer, G(N2-H)_{syn}[•]; ^b PCM solvation model; ^cRelative stabilities calculated by us by substituting methyl (CH₃) group at the N9 site of the guanine radical in the presence of a single water molecule placed between N1 and N2 side of the 9-methyl guanine radical; ^dThe solvation free energies using COSMO model are given in the parentheses; ^eEnthalpy calculated at 0K; ^f Car-Parrinello molecular dynamics (CPMD) method; ^g Zero-point vibration corrected energies. (Reprinted with permission from ref. [189], J. Phys. Chem. © (2006) American Chemical Society.)

ESR experimental hyperfine couplings. This shows the inadequacy in choosing the theoretical model which does not take into account the full solvation effects.

Since our model appeared to be inadequate to match experiment, we increased our level of modeling and incorporated seven water molecules around the guanine moiety to take into account, the effect of the first hydration shell. The geometries of G^{*+}+7H₂O, G(N1-H)[•]+7H₂O and G(N2-H)_{syn}[•]+7H₂O were fully optimized using B3LYP/6-31G(d) method [189]. These calculations indicate that G(N1-H)[•]+7H₂O is more stable than the G(N2-H)_{syn}[•]+7H₂O by 3.26 kcal/mol (see Table 20-11). The effect of bulk water was also considered through the PCM model at B3LYP/6-31G(d) level of theory. These PCM calculations still show that G(N1-H)[•]+7H₂O is more stable than the G(N2-H)_{syn}[•]+7H₂O by 3.00 kcal/mol (Table 20-11). The total hydrogen bond energies of G(N1-H)[•]+7H₂O and G(N2-H)_{syn}[•]+7H₂O were summed and found to be -104.1 kcal/mol and -95.6 kcal/mol, respectively. This shows stronger hydrogen bonding in G(N1-H)[•]+7H₂O than G(N2-H)_{syn}[•]+7H₂O account for the increased stability of this tautomer on hydration. Note that each system has same number of hydrogen bonds only the strength of the bonds differ, for details see ref. [189].

The HFCCs of G^{*+}+7H₂O, G(N1-H)[•]+7H₂O and G(N2-H)_{syn}[•]+7H₂O were calculated using the B3LYP/6-31G(d) method. We found that the calculated HFCCs with seven water molecules match very well with experiment [189], see Table 20-12. However, for G(-2H)^{•-} the match to experiment was best with 8-10 water molecules. This study clearly predicts that the G(N1-H)[•] tautomer is most

Table 20-12. Experimental and Theoretical^a ESR Parameters for $G^{\bullet+}$, $G(-H)^{\bullet}$ and $G(-2H)^{\bullet-}$

Radical	8-D-dGuo/dGuo ^b			dGuo			8-D-dGuo/dGuo				
	¹⁴ N _z	¹⁴ N _{xx}	¹⁴ N _{yy}	¹⁴ N _z	¹⁴ N _{xx}	¹⁴ N _{yy}	¹⁴ N _z	¹⁴ N _{xx}	¹⁴ N _{yy}	g-values (experimental)	
$G^{\bullet+}$	Exp ^{c,d,e}	13.0	~0	~0	6.5	~0	~0	-7.5	-10.5	-3.5	$g_{xx} = 2.0045$
	Theory										$g_{yy} = 2.0045$
$G^{\bullet+} + 7 H_2O$	Exp ^{c,d,e}	11.8	0.8	0.8	9.1	0.6	0.6	-7.8	-10.4	-2.4	$g_{zz} = 2.0021$
	Theory										
$G(-H)^{\bullet}$	Exp ^{c,d,e}	12.0	~0	~0	8.0	~0	~0	-7.2	-10.5	-3.5	$g_{xx} = 2.0041$
	Theory										$g_{yy} = 2.0041$
$G(N1-H)^{\bullet} + 7 H_2O$	Exp ^{c,d,e}	13.5	0.8	0.9	9.1	0.6	0.7	-8.4	-11.3	-3.0	$g_{zz} = 2.0021$
	Theory										
$G(N2-H)^{\bullet} + 7 H_2O$	Exp ^{c,d,e}	15.0	1.0	1.0	17.6	0.8	0.8	-6.6	-8.8	-2.3	
	Theory										
$G(-2H)^{\bullet-}$	Exp ^{c,d,e}	13.2	~0	~0	16.2	~0	~0	-5.5	-7.5	-2.5	$g_{xx} = 2.0042$
	Theory										$g_{yy} = 2.0042$
$G(-2H)^{\bullet-} + 9 H_2O$	Exp ^{c,d,e}	14.8	0.9	1.0	17.6	0.8	0.8	-6.8	-9.3	-2.6	$g_{zz} = 2.0025$
	Theory										
$G(-2H)^{\bullet-} + 10 H_2O$	Exp ^{c,d,e}	15.1	1.0	1.0	15.5	0.7	0.7	-7.2	-9.8	-2.7	
	Theory										

^a Structures optimized and hyperfine couplings calculated using B3LYP/6-31G(d) method. The theoretical models that matched experiment best are shown in bold; ^b Experimental nitrogen hyperfine couplings and g values were measured in 8-D-dGuo and these were then employed to simulate the spectra of $G^{\bullet+}$, $G(-H)^{\bullet}$ and $G(-2H)^{\bullet-}$ in dGuo; ^c Experimental A_{xx} and A_{yy} nitrogen hyperfine couplings of value ca. zero are within the line-width and too small to be characterized. Theoretical values confirm the small values of these couplings; ^d Line-shapes used were generally Lorentzian for the 8-D-dGuo and Gaussian for dGuo radical species. The C8(H) coupling creates a superposition of line components at various orientations best simulated with the Gaussian lineshape; ^e¹⁵N (spin= 1/2) couplings are 1.404 times the nitrogen couplings (¹⁴N, spin= 1) shown above. (Reprinted with permission from ref. [189], J. Phys. Chem. © (2006) American Chemical Society.)

stable in an aqueous environment and confirms that the N1-H site is the preferred deprotonation site of $G^{\bullet+}$ in an aqueous medium. This study shows that while the PCM model considers the effect of bulk solvent, it lacks important interactions between solute and solvent which can as in this case determine the most stable state. Using pulse radiolysis and theoretical modeling, Chatgililoglu et al. [190] suggested that $G^{\bullet+}$ first decays to $G(N2-H)^{\bullet}$ which undergoes water assisted tautomerization to $G(N1-H)^{\bullet}$. However, our experimental ESR study and theoretical calculations [189] suggest that the $G(N1-H)^{\bullet}$ tautomer likely is formed directly without an intermediate. We note, it is clear that in nonaqueous environments such as single crystals of nucleosides, that both theory and experiment agree that the $G(N2-H)^{\bullet}$ is the more stable tautomer.

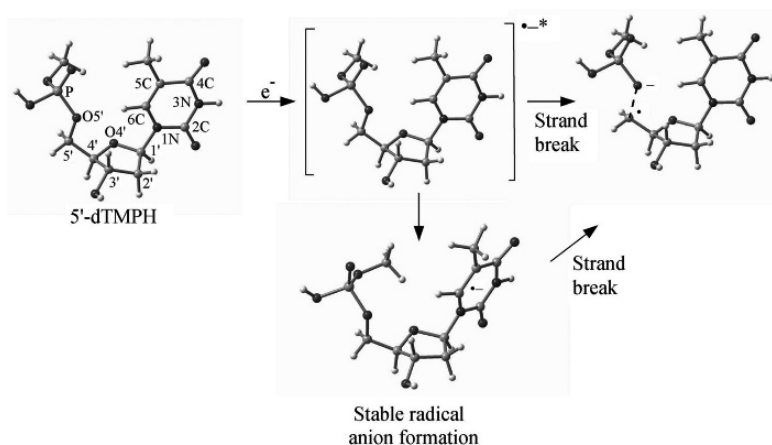
20.5. LOW ENERGY ELECTRON (LEE) ATTACHMENT AND MECHANISM OF STRAND BREAKS

The interaction of radiation with DNA leading to damage has been extensively studied with the goal of understanding the detailed mechanisms of damage within living cells at a molecular level [1–6, 59, 60, 182]. The recent discovery made by Sanche's group [11–15, 191, 192] that low energy electrons (LEEs), below 4 eV, are able to produce strand breaks in DNA attracted intense interest as it represented a new mechanism for strand break formation in DNA. Sanche and co-workers [192] showed that LEEs below DNA ionization thresholds induce strand breaks. Recently, experiments confirm that LEEs within the sub-excitation energy range 0.1–3 eV leads to a variety of chemical reactions in DNA and its components [9]. These involve: hydrogen atom loss from DNA bases [9], single-strand breaks (SSBs) [11, 12, 192], glycosidic bond cleavage [12, 15] and the fragmentation of deoxyribose [129]. It is believed that LEEs initially captured by the DNA components (bases, phosphate, deoxyribose) form transient negative ions (TNI) leading to dissociative electron attachment (DEA) [11–15, 192] mechanism.

Recently, several groups have investigated the LEE induced strand breaks via experiment [11–15, 128–131, 136, 139, 193]. In addition, a variety of theoretical papers have presented models exploring the mechanism for LEE induced SSB [194–205]. The first model of strand break formation was proposed by Simons and co-workers [196–201]. They proposed an “electron induced” indirect mechanism of action [196–201] for $C_{5'}-O_{5'}$ sugar-phosphate bond dissociation in 5'-dTMP and 5'-dCMP model systems. In this model, the electron is initially captured into a π^* molecular orbital (shape resonance) of the pyrimidine base in 5'-dTMP and 5'-dCMP and on C-O bond elongation electron transfer to the $C_{5'}-O_{5'}$ bond in sugar phosphate group bond cleavage results [196]. Li et al. [195], presented an alternative mechanism of direct electron addition to the sugar phosphate resulting in C-O sugar-phosphate bond dissociation. They used B3LYP/6-31+G(d) and ONIOM methods on a sugar-phosphate-sugar (S-P-S) model without DNA bases. Li et al. calculated a barrier height of ~ 10.0 kcal/mol for the dissociation of the C-O bond at both the 3'- and 5'- sites. Recently, they showed the spin density distribution

of the excess electron in the initial state was not a valence bound but a “dipole bound” anionic state. Thus, their model gives the dissociation of C-O bond cleavage from a weakly associated electron that is captured at the transition state into a σ^* dissociative surface. Recently, using B3LYP/DZP++ level of theory, Leszczynski and co-workers [203, 204] calculated the dissociation of $C_{5'}-O_{5'}$ and $C_{3'}-O_{3'}$ bond dissociation in pyrimidine nucleotides anion radicals. As expected they also find the initial localization of the excess electron in the π^* orbital of the base, which, subsequently transfers to the σ^* orbital of the C-O bond at transition state as proposed by Simons and co-workers [196–201]. In Scheme 20-3 we show the proposed mechanism of electron induced single strand break (SSB) for the 5'-thymidine mono-phosphate (5'-dTMPH) model system.

Recently, Märk, Illenberger and co-workers [129, 206, 207] studied the decomposition of D-ribose [129], thymidine [206] and phosphoric acid esters [207] by low energy electrons (LEEs) and showed the migration of the excess electron from the π^* orbital of the anion of the nucleobase to DNA backbone is inhibited and may hence not contribute to SSBs as proposed by Simons et al. [196–201]. They [129, 206, 207] also proposed that the direct mechanism of SSBs occurring in DNA at subexcitation energy (< 4 eV) is due to dissociative electron attachment (DEA) directly to the phosphate group [207]. Further, they [207] suggested that LEE may be trapped into the virtual molecular orbital (MO) of the phosphate group which is characterized as “shape resonance”. The “shape resonance” or “single particle resonance” occurs at low energy (0–4 eV) and has the life time of 10^{-10} – 10^{-15} sec and has several pathways to decay, such as, vibrational and rotational levels of molecule, electronic excitation, elastic scattering and dissociative electron attachment (DEA) [208]. Sanche et al. [12], also, found the formation of well



Scheme 20-3. Proposed mechanism of single strand break (SSB) due to attachment of LEE with 5'-dTMPH molecule. (Reprinted with permission from [209], J. Phys. Chem. © (2007) American Chemical Society.)

localized transient anionic state (resonance) in plasmid DNA which leads to SSBs and DSBs.

Thus from the above discussion, it is apparent that the theoretical models of strand break (indirect mechanism) as proposed by Simons et al. [196–201] and Leszczynski et al. [203, 204] as well as the direct mechanism of Li et al. [195] were helpful but suggested a need for further investigation [12, 129, 206, 207]. With this in mind, we [209] recently studied the $C_{5'}-O_{5'}$ bond dissociation in 5'-dTMPH using B3LYP method and 6-31G* and 6-31++G** basis sets, respectively. In this study [209], single strand breaks (SSB) resulting from LEE attachment to a model for DNA (5'-dTMPH) were investigated but differed from the previous studies on 5'-dTMPH in the following aspects: (i) the potential energy surfaces (PESs) of $C_{5'}-O_{5'}$ bond dissociation due to LEE attachment was investigated along the vertical as well as the adiabatic surfaces. (ii) After electron attachment to the neutral 5'-dTMPH, the vertical surface was followed by elongation of the $C_{5'}-O_{5'}$ bond elongation while maintaining the remainder of the structure in the neutral optimized geometry. (iii) The singly occupied molecular orbital (SOMO) was also followed with the elongation to note where the electron moves from the base to the sugar phosphate $C_{5'}-O_{5'}$ bond region. The first few unoccupied molecular orbitals (UMOs) energies and their nature were also investigated in the neutral molecule. In this study, it was also found that 6-31G* and 6-31++G** basis sets gave similar activation energetics (14.8 and 13.5 kcal/mol) for adiabatic bond cleavage as DZP++ basis set (13.8 kcal/mol) used in earlier studies [203–204].

In Figure 20-5, we present the first five UMOs including the highest occupied molecular orbital (HOMO) of neutral 5'-dTMPH molecule. Their orbital energies in eV, calculated using B3LYP/6-31G* method, are also presented in Figure 20-5. We found that B3LYP/6-31G* method predicts two lowest π^* orbitals having energies (in eV) $-0.84(\pi_1^*)$ and $0.43(\pi_2^*)$, respectively, and three lowest σ^* orbitals having energies $0.73(\sigma_1^*)$, $1.27(\sigma_2^*)$ and $1.78(\sigma_3^*)$. From Figure 20-5, it is clearly evident that π^* orbitals are localized on the thymine base while σ^* orbitals are localized on the sugar-phosphate groups and particularly the σ_1^* orbital is localized on the phosphate group. It is also well established that within Koopmans' theorem approximation, the vertical attachment energies (VAEs) are equal to the virtual orbital energies (VOEs) but at the Hartree-Fock (HF) and DFT level of theories these VOEs are overestimated by several eVs and need scaling to appropriately represent the experimental VAEs [33, 85, 210–216]. Thus using the scaling equation as used by Modelli [215], we obtained the scaled VOEs of corresponding B3LYP/6-31G* computed LUMOs of 5'-dTMPH as $0.53(\pi_1^*)$, $1.56(\pi_2^*)$, $1.80(\sigma_1^*)$, $2.23(\sigma_2^*)$ and $2.64(\sigma_3^*)$ eV, respectively [209]. Using electron transmission spectroscopy (ETS), Aflatooni et al. [94] reported the two lowest π^* orbital VAEs of thymine as 0.29 and 1.71 eV, respectively, which are in close agreement to our calculated values [209], see Figure 20-5. From scaled VOEs, it is clear that even below 2 eV the LUMOs on the phosphate group as well as on the bases are available for LEE attachment. This important aspect has not been studied in the earlier studies [195–201, 203, 204].

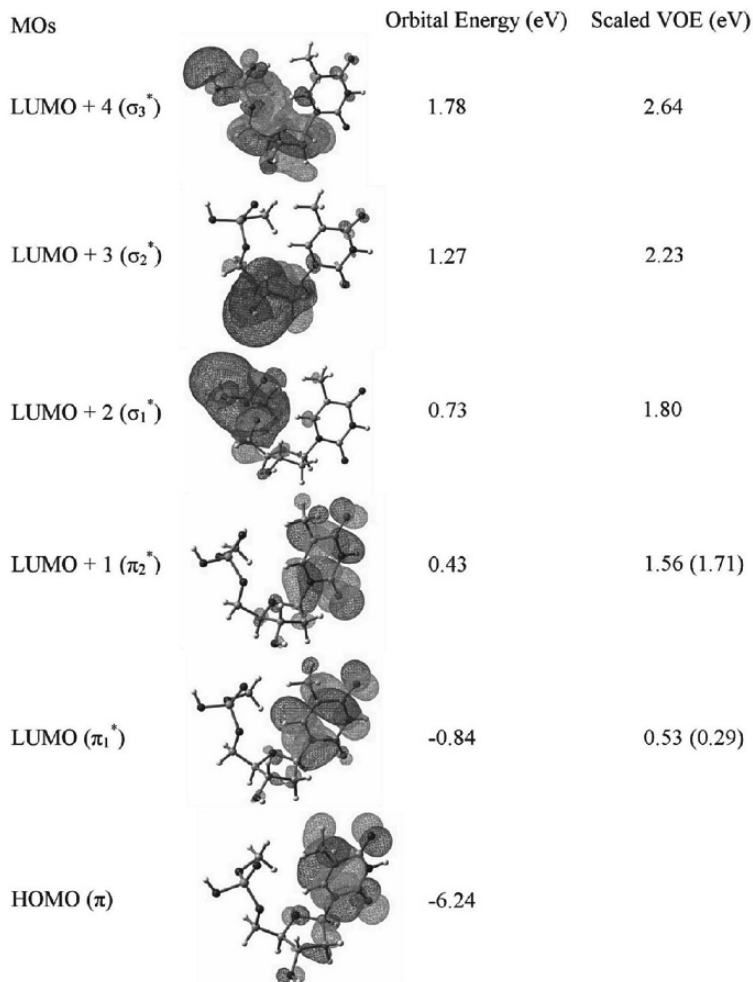


Figure 20-5. Molecular orbital plots of neutral 5'-dTMPH, calculated using the B3LYP/6-31G* method. B3LYP/6-31G* calculated orbital energies along with scaled values are given in eV. In parentheses the experimental VOEs of thymine (Ref. [94]) are given in eV. (Reprinted with permission from ref. [209], J. Phys. Chem. © (2007) American Chemical Society.)

As pointed out above, in order to elucidate the mechanism of single strand break (SSB), we scanned the adiabatic and vertical PESs by stretching the $C_{5'}-O_{5'}$ bond from the equilibrium bond length of neutral and anion radical of 5'-dTMPH up to 2 Å in the step of 0.1 Å using B3LYP/6-31G* and B3LYP/6-31++G** methods, respectively. The corresponding PESs of $C_{5'}-O_{5'}$ bond dissociation using both of these methods are shown in Figures 20-6 and 20-7, respectively, for a detail description, see ref. [209]. From Figures 20-6 and 20-7, we found that on

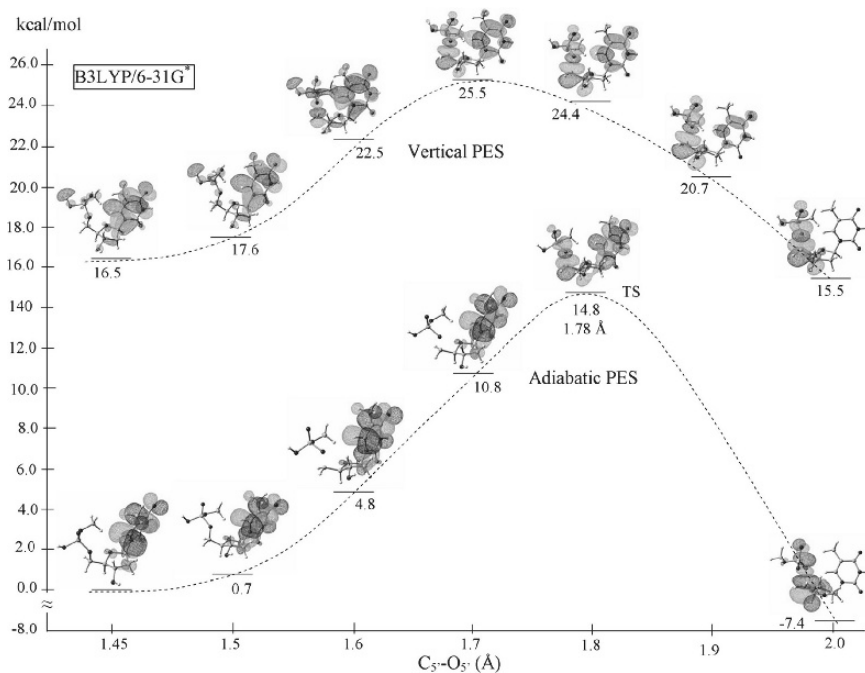


Figure 20-6. B3LYP/6-31G* calculated adiabatic and vertical potential energy surfaces (PESs) of $C_{5'}$ - $O_{5'}$ bond dissociation of 5'-dTMPH radical anion. Energies and distances are given in kcal/mol and angstroms (Å), respectively. The singly occupied molecular orbital (SOMO) is also shown. (Reprinted with permission from ref. [209], J. Phys. Chem. © (2007) American Chemical Society.)

the adiabatic surfaces both the methods predict the similar barrier height of $C_{5'}$ - $O_{5'}$ bond dissociation and the SOMOs are localized on the thymine base and transfer only at the transition state (TS) of the $C_{5'}$ - $O_{5'}$ bond dissociation. On the vertical PES, the B3LYP/6-31G* calculated barrier height is found to be ~ 9 kcal/mol which is actually lower than the adiabatic value while the corresponding value calculated using B3LYP/6-31++G** method is found to be ~ 17 kcal/mol. Interestingly, we found that in vertical state excess electron begins transferring into the $C_{5'}$ - $O_{5'}$ bond region on bond elongation before the TS while in the adiabatic state no electron transfer into the $C_{5'}$ - $O_{5'}$ bond region is found below the TS. This suggests that the indirect mechanism for SSB is unlikely along the adiabatic pathway. The result for the vertical PES provides some support for the hypothesis that transiently bound electron (shape resonance) to the virtual molecular orbitals of the neutral molecule play a role in the cleavage of the sugar-phosphate C-O bond in DNA resulting in the direct formation of SSBs without significant molecular relaxation. In this regard, the works of Burrow et al. [85, 94, 216] and Sanche et al. [217], it is clear that LEE attachment can excite specific vibrational modes even in the condensed phase [217]. Therefore, it is quite possible that LEEs may excite vibrational modes which

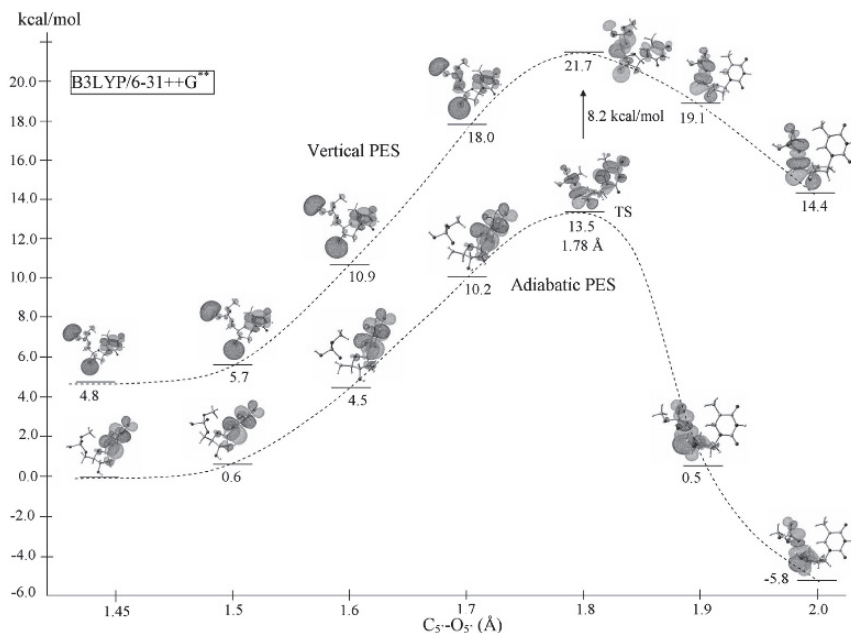


Figure 20-7. B3LYP/6-31++G** calculated adiabatic and vertical potential energy surfaces (PESs) of $C_{5'}-O_{5'}$ bond dissociation of 5'-dTMPH radical anion. Energies and distances are given in kcal/mol and angstroms (Å), respectively. The singly occupied molecular orbital (SOMO) is also shown. (Reprinted with permission from ref. [209], J. Phys. Chem. © (2007) American Chemical Society.)

directly lead to bond elongation and bond dissociation which for some pathways would have low barriers as found in our present work [209]. Also, on the time scale the transition state and specific vibrational motions will dominate at $<10^{-12}$ s [218]. Thus, if on LEE attachment transient anion formation results in vibrationally excitation of the $C_{5'}-O_{5'}$ bond then the bond dissociation process will proceed with only a small barrier. Our results also predict the availability of states on the phosphate group at less than 2 eV [209] (see Figure 20-5). This possibility has, also, been reported in the experimental work by Caron and Sanche [219–221] and Märk, Illenberger and co-workers [129, 207] as well as a number of theoretical studies [195, 196].

20.6. CONCLUSIONS

High energy radiation damage results in unstable reactive intermediates localized to specific portions of DNA. The energetic nature of these species makes them, particularly, accessible to high level theoretical calculations since the subsequent mechanistic processes are driven by sizeable energetic driving forces. For this reason, theoretical calculations are likely to have substantial predictive power and combined with insightful approaches can lead to a detailed understanding of the

radiation induced mechanisms on a molecular scale. In this review results of literally hundreds of works establish the predictive power of the theoretical approach and have firmly established the beginnings of our understanding of radiation effects on DNA. Especially noteworthy are the recent theoretical support for low energy electrons in the production of DNA strand breaks, the role of excited states of holes in the production of sugar radicals and the preferred deprotonation sites in deoxyguanosine cation radical ($G^{\bullet+}$). In the future, we look forward to further treatment of these interesting problems and developments in theory that allow for facile treatment of potential energy surfaces for anion and cation excited states.

ACKNOWLEDGMENTS

This work was supported by the NIH NCI under grant no. R01CA045424. The authors are also grateful to the Arctic Region Supercomputing Center (ARSC) for generously providing the computational time to perform these calculations. The authors also thank the ARSC staff for their support and cooperation. We also thank Prof. D. Becker, Dr. A. Adhikary, S. Collins and D. Kanduri for aid and helpful discussions.

REFERENCES

1. Sevilla MD, Becker D (2004) ESR studies of radiation damage to DNA and related biomolecules. In: Royal Society of Chemistry Special Periodical Report, Electron Spin Resonance, London, Vol. 19, p 243.
2. Becker D, Sevilla MD (1993) The chemical consequences of radiation damage to DNA. In: Lett J (ed.) *Advances in Radiation Biology*, Vol. 17, Academic Press, New York, p 121.
3. Burrows CJ, Muller JG (1998) *Chem Rev* 98:1109.
4. von Sonntag C (1991) The chemistry of free-radical-mediated DNA damage. In: Glass WA, Varma MN (eds.) *Physical and Chemical Mechanisms in Molecular Radiation Biology*, Plenum, New York, p 287.
5. Swarts SG, Sevilla MD, Becker D, Tokar CJ, Wheeler KT (1992) *Radiat Res* 129: 333.
6. Swiderek P (2006) *Angew Chem Int Ed* 45:4056.
7. Xifeng Li, Sevilla MD (2007) *Adv Quantum Chem* 52:59.
8. Becker D, Adhikary A, Sevilla MD (2007) The Role of Charge and Spin Migration in DNA Radiation Damage. In *Charge Migration in DNA* (Chakraborty T(ed.)), Springer-Verlag, Berlin, Heidelberg, p 139.
9. Hanel G, Gstir B, Denifl S, Scheier P, Probst M, Farizon B, Farizon M, Illenberger E, Märk TD (2003) *Phys Rev Lett* 90:188104.
10. Pimblott SM, Laverne JA, Mozumber A (1996) *J Phys Chem* 100:8595.
11. Boudaïffa B, Cloutier P, Hunting D, Huels MA, Sanche L (2000) *Science* 287:1658.
12. Huels MA, Boudaïffa B, Cloutier P, Hunting D, Sanche L (2003) *J Am Chem Soc* 125:4467.
13. Sanche L (2005) *Eur Phys J D* 35:367.
14. Zheng Y, Cloutier P, Hunting DJ, Sanche L, Wagner JR (2005) *J Am Chem Soc* 127:16592.
15. Zheng Y, Wagner JR, Sanche L (2006) *Phys Rev Lett* 96:208101.

16. Abdoul-Carime H, Dugal PC, Sanche L (2000) *Radiat Res* 153:23.
17. Yan MY, Becker D, Summerfield S, Renke P, Sevilla MD (1992) *J Phys Chem* 96:1983.
18. Cai ZL, Sevilla MD (2004) *Topics in Current Chemistry* 237:103.
19. Schuster GB (2000) *Acc Chem Res* 33:253.
20. Schuster GB (ed.) (2004) *Topics in Current Chemistry Vol 236*, Springer-Verlag, Berlin, Heidelberg.
21. Schuster GB (ed.) (2004) *Topics in Current Chemistry Vol 237*, Springer-Verlag, Berlin, Heidelberg.
22. Wang W, Becker D, Sevilla MD (1993) *Radiat Res* 135:146.
23. Steenken S, Jovanovic SV (1997) *J Am Chem Soc* 119:617.
24. Bixon M, Jortner J (2000) *J Phys Chem B* 104:3906.
25. Saito I, Takayama M, Sugiyama H, Nakatani K, Tsuchida A, Yamamoto M (1995) *J Am Chem Soc* 117:6406.
26. Swarts SG, Becker D, Sevilla MD, Wheeler KJ (1996) *Radiat Res* 146:304.
27. Becker D, Bryant-Friedrich A, Trzasko C, Sevilla MD (2003) *Radiat Res* 160:174.
28. Becker D, Razskazovskii Y, Callaghan MU, Sevilla MD (1996) *Radiat Res* 146: 361.
29. Shukla LI, Pazdro R, Huang J, DeVreugd C, Becker D, Sevilla MD (2004) *Radiat Res* 161:582.
30. Shao Y, Molnar LF, Jung Y, Kussmann J, Ochsenfeld C, Brown ST, Gilbert ATB, Slipchenko LV, Levchenko SV, O'Neill DP, DiStasio RA, Lochan RC, Wang T, Beran GJO, Besley NA, Herbert JM, Lin CY, Van Voorhis T, Chien SH, Sodt A, Steele RP, Rassolov VA, Maslen PE, Korambath PP, Adamson RD, Austin B, Baker J, Byrd EFC, Dachsel H, Doerksen RJ, Dreuw A, Dunietz BD, Dutoi AD, Furlani TR, Gwaltney SR, Heyden A, Hirata S, Hsu CP, Kedziora G, Khallulin RZ, Klunzinger P, Lee AM, Lee MS, Liang W, Lotan I, Nair N, Peters B, Proynov EI, Pieniazek PA, Rhee YM, Ritchie J, Rosta E, Sherrill CD, Simmonett AC, Subotnik JE, Woodcock HL, Zhang W, Bell AT, Chakraborty AK, Chipman DM, Keil FJ, Warshel A, Hehre WJ, Schaefer HF, Kong J, Krylov AI, Gill PMW, Head-Gordon M (2006) *Phys Chem Chem Phys* 8:3172.
31. Alberts I (1999) *Annu Rep Prog Chem B* 95:373.
32. Sevilla MD, Becker D, Yan M, Summerfield SR (1991) *J Phys Chem* 95:3409.
33. Sevilla MD, Besler B, Colson AO (1995) *J Phys Chem* 99:1060.
34. Russo N, Toscano M, Grand A (2000) *J Comput Chem* 21:1243.
35. Wetmore SD, Boyd RJ, Eriksson LA (2000) *Chem Phys Lett* 322:129.
36. Rubio M, Roca-Sanjuán D, Merchán M, Serrano-Andrés L (2006) *J Phys Chem B* 110:10234.
37. Tureèk F (2007) *Adv Quantum Chem* 52:89.
38. Cauët E, Dehareng D, Liévin J (2006) *J Phys Chem A* 110:9200.
39. Crespo-Hernandez CE, Arce R, Ishikawa Y, Gorb L, Leszczynski J, Close DM (2004) *J Phys Chem A* 108:6373.
40. Zakjevskii VV, King SJ, Dolgounitcheva O, Zakrzewski VG, Ortiz JV (2006) *J Am Chem Soc* 128:13350.
41. Orlov VM, Smirnov AN, Varshavsky YM (1976) *Tetrahedron Lett* 48:4377.
42. Hush NS, Cheung AS (1975) *Chem Phys Lett* 34:11.
43. Yang X, Wang XB, Vorpagel ER, Wang LS (2004) *Proc Natl Acad Sci USA* 101:17588.
44. Fernando H, Papadantonakis GA, Kim NS, LeBreton PR (1998) *Proc Natl Acad Sci USA* 95:5550.
45. Close DM (2004) *J Phys Chem A* 108:10376.
46. Colson AO, Besler B, Sevilla MD (1992) *J Phys Chem* 96:9787.
47. (a) Li XF, Cai ZL, Sevilla MD (2002) *J Phys Chem A* 106:9345; (b) Li XF, Cai ZL, Sevilla MD (2001) *J Phys Chem B* 105:10115.
48. Hutter M, Clark T (1996) *J Am Chem Soc* 118:7574.

49. Bertran J, Oliva A, Rodriguez-Santiago L, Sodupe M (1998) *J Am Chem Soc* 120:8159.
50. Giese B, Amaudrut J, Kohler A, Sportmann MAWS (2001) *Nature* 412:318.
51. Sartor V, Boone E, Schuster GB (2001) *J Phys Chem B* 105:11057.
52. Kawai K, Osakada Y, Fujitsuka M, Majima T (2007) *J Phys Chem B* 111:2322.
53. Colson AO, Sevilla MD (1995) *Int J Radiat Biol* 67:627.
54. Colson AO, Besler B, Sevilla MD (1993) *J Phys Chem* 97:13852.
55. Barnett RN, Cleveland CL, Joy A, Landman U, Schuster GB (2001) *Science* 294:567.
56. Hutter MC (2006) *Chem Phys* 326:240.
57. Prat F, Houk KN, Foote CS (1998) *J Am Chem Soc* 120:845.
58. Sugiyama H, Saito I (1996) *J Am Chem Soc* 118:7063.
59. (a) Steenken S (1989) *Chem Rev* 89:503; (b) Steenken S, Telo JP, Novais HM, Candeias LP (1992) *J Am Chem Soc* 114:4701.
60. Steenken S (1997) *Biol Chem* 378:1293.
61. Weatherly SC, Yang IV, Thorp HH (2001) *J Am Chem Soc* 123:1236.
62. Shafirovich V, Dourandin A, Luneva NP, Geacintov NE (2000) *J Phys Chem B* 104:137.
63. Shafirovich V, Dourandin A, Huang W, Luneva NP, Geacintov NE (1999) *J Phys Chem B* 103:10924.
64. Kohen A, Klinman JP (1998) *Acc Chem Res* 31:397.
65. Colson AO, Besler B, Close DM, Sevilla MD (1992) *J Phys Chem* 96:661.
66. Schuster GB (2000) *Acc Chem Res* 33:253.
67. Giese B, Wessely S (2001) *Chem Commun* 20:2108.
68. Shafirovich V, Dourandin A, Geacintov NE (2001) *J Phys Chem B* 105:8431.
69. Gervasio FL, Boero M, Laio A, Parrinello M (2005) *Phys Rev Lett* 94:158103.
70. (a) Hammes-Schiffer S (2001) *Acc Chem Res* 34:273; (b) Skone JH, Soudackov AV, Hammes-Schiffer S (2006) *J Am Chem Soc* 128:16655.
71. Gervasio FL, Boero M, Parrinello M (2006) *Angew Chem Int Ed* 45:5606.
72. Nir E, Kleinermanns K, deVries MS (2000) *Nature* 408:949.
73. Atkins PW (1982) *Physical Chemistry*, Oxford University Press: Oxford.
74. Yanson IK, Teplitsky AB, Sukhodub LF (1979) *Biopolymers* 18:1149.
75. (a) Jurečka P, Šponer J, Černý J, Hobza P (2006) *Phys Chem Chem Phys* 8:1985; (b) Šponer J, Leszczynski J, Hobza P (1996) *J Phys Chem* 100:1965; (c) Guerra CF, Bickelhaupt FM, Snijders JG, Baerends EJ (2000) *J Am Chem Soc* 122:4117.
76. Hesselmann A, Jansen G, Schütz M (2006) *J Am Chem Soc* 128:11730.
77. Reynisson J, Steenken S (2002) *Phys Chem Chem Phys* 4:5346.
78. Reynisson J, Steenken S (2002) *Phys Chem Chem Phys* 4: 5353.
79. Svozil D, Jungwirth P, Havlas Z (2004) *Collect Czech Chem Commun* 69:1395.
80. Desfrancois C, Carles S, Schermann JP (2000) *Chem Rev* 100:3943.
81. Desfrancois C, Periquet V, Bouteiller Y, Schermann JP (1998) *J Phys Chem A* 102:1274.
82. Vera DMA, Pierini AB (2004) *Phys Chem Chem Phys* 6:2899.
83. Galbrath JM, Schaefer HF (1996) *J Chem Phys* 105:862.
84. Rösch N, Trickey SB (1997) *J Chem Phys* 106:8940.
85. Jordan KD, Burrow PD (1987) *Chem Rev* 87:557.
86. Falcetta MF, Jordan KD (1990) *J Phys Chem* 94:5666.
87. Li XF, Cai ZL, Sevilla MD (2002) *J Phys Chem A* 106:1596.
88. Li XF, Sevilla MD, Sanche L (2004) *J Phys Chem B* 108:19013.
89. Wesolowski SS, Leininger ML, Pentchev PN, Schaefer HF (2001) *J Am Chem Soc* 123:4023.
90. Falcetta MF, Choi Y, Jordan KD (2000) *J Phys Chem A* 104:9605.
91. Wang W, Yan M, Becker D, Sevilla MD (1993) *Radiat Res* 137:2.

92. Wang W, Sevilla MD (1994) *Radiat Res* 138:9.
93. Sevilla MD, Mohan P (1974) *Int J Radiat Biol* 25:635.
94. Aflatooni K, Gallup GA, Burrow PD (1998) *J Phys Chem A* 102:6205.
95. (a) Hendricks JH, Lyapustina SA, de Clercq HL, Snodgrass JT, Bowen KH (1996) *J Chem Phys* 104:7788 ; (b) Hendricks JH, Lyapustina SA, de Clercq HL, Snodgrass JT, Bowen KH (1998) *J Chem Phys* 108:8.
96. Haranczyk M, Gutowski M (2005) *J Am Chem Soc* 127:699.
97. Svozil D, Frigato T, Havlas Z, Jungwirth P (2005) *Phys Chem Chem Phys* 7:84.
98. Periquet V, Moreau A, Carles S, Schermann JP, Desfrancois C (2000) *J Electron Spectrosc Relat Phenom* 106:141.
99. Schiedt J, Weinkauff R, Neumark DM, Schlag EW (1998) *Chem Phys* 239:511.
100. Mazurkiewicz K, Bachorz RA, Gutowski M, Rak J (2006) *J Phys Chem B* 110:24696.
101. Radisic D, Bowen KH, Dabkowska I, Storoniak P, Rak J, Gutowski M (2005) *J Am Chem Soc* 127:6443.
102. Richardson NA, Wesolowski SS, Schaefer HF (2003) *J Phys Chem B* 107:848.
103. Gu JD, Xie YM, Schaefer HF (2005) *J Phys Chem B* 109:13067.
104. Kumar A, Knapp-Mohammady M, Mishra PC, Suhai S (2004) *J Comput Chem* 25:1047.
105. Richardson NA, Wesolowski SS, Schaefer HF (2002) *J Am Chem Soc* 124:10163.
106. Kumar A, Mishra PC, Suhai S (2005) *J Phys Chem A* 109:3971.
107. Rejnek J, Hanus M, Kabeláč M, Ryjáček F, Hobza P (2005) *Phys Chem Chem Phys* 7:2006.
108. Chandra AK, Nguyen MT, Zeegers-Huyskens T (1998) *J Phys Chem A* 102:6010.
109. Di Laudo M, Whittleton SR, Wetmore SD (2003) *J Phys Chem A* 107:10406.
110. Hu X, Li H, Liang W, Han SJ (2004) *J Phys Chem B* 108:12999.
111. Hu X, Li H, Liang W, Han SJ (2005) *J Phys Chem B* 109:5935.
112. Shishkin OV, Gorb L, Leszczynski J (2000) *J Phys Chem B* 104:5357; (b) Sukhanov OS, Shishkin OV, Gorb L, Podolyan Y, Leszczynski J (2003) *J Phys Chem B* 107:2846.
113. Gaigeot MP, Sprik M (2004) *J Phys Chem B* 108:7458.
114. Giudice E, Várnai P, Lavery R (2003) *Nucleic Acids Res* 31:1434.
115. Sevilla MD, Besler B, Colson AO (1994) *J Phys Chem* 98:2215.
116. Frigato T, Svozil D, Jungwirth P (2006) *J Phys Chem A* 110:2916.
117. Kim S, Schaefer HF (2006) *J Chem Phys* 125:144305.
118. Kim S, Wheeler SE, Schaefer HF (2006) *J Chem Phys* 124:204310.
119. Kim S, Schaefer HF (2007) *J Chem Phys* 126:064301.
120. Gu JA, Xie YM, Schaefer HF (2006) *Chem Phys Chem* 7:1885.
121. Gu JA, Xie YM, Schaefer HF (2006) *J Phys Chem B* 110:19696.
122. Harańczyk M, Gutowski M (2005) *Angew Chem Int Ed* 44:6585.
123. Bao XG, Sun H, Wong NB, Gu JD (2006) *J Phys Chem B* 110:5865.
124. Bao XG, Liang GM, Wong NB, Gu J (2007) *J Phys Chem A* 111:666.
125. Liu B, Tomita S, Rangama J, Hvelplund P, Nielsen SB (2003) *Chem Phys Chem* 4:1341.
126. Li XF, Sevilla MD, Sanche L (2003) *J Am Chem Soc* 125:8916.
127. Ptašínska S, Denifl S, Scheier P, Märk TD (2004) *J Chem Phys* 120:8505.
128. Denifl S, Ptašínska S, Probst M, Hrušák J, Scheier P, Märk TD (2004) *J Phys Chem A* 108:6562.
129. Bald I, Kopyra J, Illenberger E (2006) *Angew Chem Int Ed* 45:4851.
130. Ptašínska S, Denifl S, Scheier P, Illenberger E, Märk TD (2005) *Angew Chem Int Ed* 44:6941.
131. Ptašínska S, Denifl S, Mróz B, Probst M, Grill V, Illenberger E, Scheier P, Märk TD (2005) *J Chem Phys* 123:124302.
132. Zamenhof S, De Giovanni R, Greer S (1958) *Nature* 181:827.
133. Ling LL, Ward JF (1990) *Radiat Res* 121:76.

134. Li XF, Sanche L, Sevilla MD (2002) *J Phys Chem A* 106:11248.
135. Huels MA, Hahndorf I, Illenberger E, Sanche L (1998) *J Chem Phys* 108:1309.
136. Abouaf R, Pommier J, Dunet H (2003) *Int J Mass Spectrosc* 226:397.
137. Abouaf R, Dunet H (2005) *Eur Phys J D* 35:405.
138. Li XF, Sanche L, Sevilla MD (2004) *J Phys Chem B* 108:5472.
139. Abdoul-Carime H, Gohlke S, Illenberger E (2004) *Phys Rev Lett* 92:168103.
140. Bera PP, Schaefer HF (2005) *Proc Natl Acad Sci USA* 102:6698.
141. Lind MC, Bera PP, Richardson NA, Wheeler SE, Schaefer HF (2006) *Proc Natl Acad Sci USA* 103:7554.
142. Zhang JD, Xie Y, Schaefer HF (2006) *J Phys Chem A* 110:12010.
143. Evangelista FA, Paul A, Schaefer HF (2004) *J Phys Chem A* 108:3565.
144. Zhang JD, Schaefer HF (2007) *J Chem Theory Comput* 3:115.
145. Luo Q, Li J, Li QS, Kim S, Wheeler SE, Xie M, Schaefer HF (2005) *Phys Chem Chem Phys* 7:861.
146. Shukla LI, Pazdro R, Becker D, Sevilla MD (2005) *Radiat Res* 163:591.
147. Adhikary A, Kumar A, Sevilla MD (2006) *Radiat Res* 165:479.
148. Adhikary A, Malkhasian AYS, Collins S, Koppen J, Becker D, Sevilla MD (2005) *Nucleic Acids Res* 33:5553.
149. Adhikary A, Becker D, Collins S, Koppen J, Sevilla MD (2006) *Nucleic Acids Res* 34:1501.
150. Alexander C. Jr, Franklin CE (1971) *J Chem Phys* 54:1909.
151. Tronche C, Goodman BK, Greenberg MM (1998) *Chem Biol* 5:263.
152. Pogozelski WK, Tullius TD (1998) *Chem Rev* 98:1089.
153. Kumar A, Sevilla MD (2006) *J Phys Chem B* 110:24181.
154. Tsolakidis A, Kaxiras E (2005) *J Phys Chem A* 109:2373.
155. Cossi M, Barone V (2001) *J Chem Phys* 115:4708.
156. Gustavsson T, Banyasz A, Lazzarotto E, Markovitsi D, Scalmani G, Frisch MJ, Barone V, Improta R (2006) *J Am Chem Soc* 128:607.
157. Shukla MK, Leszczynski J (2004) *J Comput Chem* 25:768.
158. Shukla MK, Leszczynski J (2002) *J Phys Chem A* 106:11338.
159. Hirata S, Head-Gordon M, Szczepanski J, Vala M (2003) *J Phys Chem A* 107:4940.
160. Halasinski TM, Weisman JL, Ruiterkamp R, Lee TJ, Salama F, Head-Gordon M (2003) *J Phys Chem A* 107:3660.
161. Hirata S, Lee TJ, Head-Gordon M (1999) *J Chem Phys* 111:8904.
162. Blancafort L, Voityuk AA (2006) *J Phys Chem A* 110:6426.
163. Dreuw A, Head-Gordon M (2005) *Chem Rev* 105:4009.
164. Dreuw A, Weisman JL, Head-Gordon M (2003) *J Chem Phys* 119:2943.
165. Voityuk AA (2005) *J Chem Phys* 122:204904.
166. Voityuk AA (2005) *J Phys Chem B* 109:10793.
167. Saito I, Nakamura T, Nakatani K, Yoshioka Y, Yamaguchi K, Sugiyama H (1998) *J Am Chem Soc* 120:12686.
168. Hall DB, Holmlin RE, Barton JK (1996) *Nature* 382:731.
169. Senthilkumar K, Grozema FC, Guerra CF, Bickelhaupt FM, Siebbeles LDA (2003) *J Am Chem Soc* 125:13658.
170. Lewis FD (2005) *Photochem Photobiol* 81:65.
171. Joy A, Ghosh AK, Schuster GB (2006) *J Am Chem Soc* 128:5346.
172. Saito I, Takayama M, Kawanishi S (1995) *J Am Chem Soc* 117:5590.
173. Jovanovic SV, Simic MG (1986) *J Phys Chem* 90:974.
174. Jovanovic SV, Simic MG (1989) *Biochim Biophys Acta* 1008:39.

175. Candeias LP, Steenken S (1989) *J Am Chem Soc* 111:1094.
176. Steenken S, Jovanovic SV, Candeias LP, Reynisson J (2001) *Chem Eur J* 7:2829.
177. Kobayashi K, Tagawa S (2003) *J Am Chem Soc* 125:10213.
178. Wetmore SD, Boyd RJ, Eriksson LA (1998) *J Phys Chem B* 102:9332.
179. Mundy CJ, Colvin ME, Quong AA (2002) *J Phys Chem A* 106:10063.
180. Gervasio FL, Laio A, Iannuzzi M, Parrinello M (2004) *Chem Eur J* 10:4846.
181. Luo Q, Li QS, Xie Y, Schaefer HF (2005) *Collect Czech Chem Commun* 70:826.
182. von Sonntag C (2006) *Free-Radical-Induced DNA Damage and Its Repair*, Springer-Verlag, Berlin, Heidelberg, pp 220–221.
183. Chatgililoglu C, Caminal C, Guerra M, Mulazzani QG (2005) *Angew Chem Int Ed* 44:6030.
184. Bachler V, Hildenbrand K (1992) *Radiat Phys Chem* 40:59.
185. Close DM, Sagstuen E, Nelson WH (1985) *J Chem Phys* 82:4386.
186. Hole EO, Sagstuen E, Nelson WH, Close DM (1991) *Radiat Res* 125:119.
187. Hole EO, Sagstuen E, Nelson WH, Close DM (1992) *Radiat Res* 129:1.
188. Hole EO, Sagstuen E, Nelson WH, Close DM (1992) *Radiat Res* 129:119.
189. Adhikary A, Kumar A, Becker D, Sevilla MD (2006) *J Phys Chem B* 110:24171.
190. Chatgililoglu C, Caminal C, Altieri A, Vougioukalakis GC, Mulazzani QG, Gimisis T, Guerra M (2006) *J Am Chem Soc* 128:13796.
191. Zheng Y, Cloutier P, Hunting DJ, Wagner JR, Sanche L (2004) *J Am Chem Soc* 126:1002.
192. Martin F, Burrow PD, Cai Z, Cloutier P, Hunting D, Sanche L (2004) *Phys Rev Lett* 93:068101.
193. Denifl S, Ptasinska S, Cingel M, Matejcek S, Scheier P, Märk TD (2003) *Chem Phys Lett* 377:74.
194. Li X, Sanche L, Sevilla MD (2006) *Radiat Res* 165:721.
195. Li X, Sevilla MD, Sanche L (2003) *J Am Chem Soc* 125:13668.
196. Simons J (2006) *Acc Chem Res* 39:772.
197. Berdys J, Anusiewicz I, Skurski P, Simons J (2004) *J Am Chem Soc* 126:6441.
198. Anusiewicz I, Berdys J, Sobczyk M, Skurski P, Simons J (2004) *J Phys Chem A* 108:11381.
199. Berdys J, Anusiewicz I, Skurski P, Simons J (2004) *J Phys Chem A* 108:2999.
200. Barrios R, Skurski P, Simons J (2002) *J Phys Chem B* 106:7991.
201. Berdys J, Skurski P, Simons J (2004) *J Phys Chem B* 108:5800.
202. Gu J, Xie Y, Schaefer HF (2005) *J Am Chem Soc* 127:1053.
203. Bao X, Wang J, Gu J, Leszczynski J (2006) *Proc Nat Acad Sci USA* 103:5658.
204. Gu J, Wang J, Leszczynski J (2006) *J Am Chem Soc* 128:9322.
205. Millen AL, Archibald LAB, Hunter KC, Wetmore SD (2007) *J Phys Chem B* 111:3800.
206. Ptasinska S, Denifl S, Gohlke S, Scheier P, Illenberger E, Märk TD (2006) *Angew Chem Int Ed* 45:1893.
207. König C, Kopyra J, Bald I, Illenberger E (2006) *Phys Rev Lett* 97:018105.
208. Schulz GJ (1973) *Rev Mod Phys* 45:423.
209. Kumar A, Sevilla MD (2007) *J Phys Chem B* 111:5464.
210. Burrow PD, Gallup GA, Scheer AM, Denifl S, Ptasinska S, Märk T, Scheier P (2006) *J Chem Phys* 124:124310.
211. Scheer AM, Silvernail C, Belot JA, Aflatooni K, Gallup GA, Burrow PD (2005) *Chem Phys Lett* 411:46.
212. Scheer AM, Aflatooni K, Gallup GA, Burrow PD (2004) *Phys Rev Lett* 92:068102.
213. Aflatooni K, Scheer AM, Burrow PD (2006) *J Chem Phys* 125:054301.
214. Staley SW, Strand JT (1994) *J Phys Chem* 98:116.
215. Modelli A (2003) *Phys Chem Chem Phys* 5:2923.
216. Jordan KD, Burrow PD (1978) *Acc Chem Res* 11:341.
217. Levesque PL, Michaud M, Sanche L (2003) *Nucl Instr Meth Phys Res B* 208:225.

218. Zewail AH (2000) *J Phys Chem A* 104:5660.
219. Caron L, Sanche L (2005) *Phys Rev A* 72:032726.
220. Mozejko P, Sanche L (2005) *Radiat Phys Chem* 73:77.
221. Pan X, Sanche L (2006) *Chem Phys Letts* 421:404.